

DRAFT VERSION MAY 23, 2023

Typeset using L^AT_EX **modern** style in AASTeX631

A possible surviving companion of the SN Ia in the Galactic SNR G272.2-3.2

P. RUIZ-LAPUENTE,^{1,2} J.I. GONZÁLEZ HERNÁNDEZ,^{3,4} R. CARTIER,⁵ K. BOUTSIA,⁶
F. FIGUERAS,^{7,2,8} R. CANAL,^{7,8} AND L. GALBANY^{9,8}

¹*Instituto de Física Fundamental, Consejo Superior de Investigaciones Científicas, c/. Serrano 121,
E-28006, Madrid, Spain*

²*Institut de Ciències del Cosmos (UB-IEEC), c/. Martí i Franqués 1, E-08028, Barcelona, Spain*

³*Instituto de Astrofísica de Canarias, E-38200 La Laguna, Tenerife, Spain*

⁴*Universidad de La Laguna, Dept. Astrofísica, E38206 La Laguna, Tenerife, Spain*

⁵*Gemini Observatory, NSF's National Optical-Infrared Research Laboratory, Casilla 603, La
Serena, Chile*

⁶*Las Campanas Observatory, Carnegie Institution for Science, Colina El Pino, Casilla 601 La
Serena, Chile*

⁷*Departament de Física Quàntica i Astrofísica, Universitat de Barcelona, c/. Martí i Franqués 1,
E-08028 Barcelona, Spain*

⁸*Institut d'Estudis Espacials de Catalunya (IEEC), E-08438, Barcelona, Spain*

⁹*Institute of Space Sciences (ICE, CSIC), Campus de Bellaterra, Can Magrans s/n, E-0893,
Bellaterra, Spain*

ABSTRACT

We use the *Gaia* EDR3 to explore the Galactic supernova remnant SNR G272.2-3.2, produced by the explosion of a Type Ia supernova (SNIa), about 7,500 years ago, to search for a surviving companion. From the abundances in the SNR ejecta, G272.2-3.2 is a normal SN Ia. The *Gaia* parallaxes allow to select the stars located within the estimated distance range of the SNR, and the *Gaia* proper motions to study their kinematics. From the *Gaia* EDR3 photometry, we construct the HR diagram of the selected sample, which we compare with the theoretical predictions for the evolution of possible star companions of SNIa. We can discard several proposed types of companions by combining kinematics and photometry. We can also discard hypervelocity stars. We focus our study on the kinematically most peculiar star, *Gaia* EDR3 5323900215411075328 (hereafter MV-G272), a 8.9 σ outlier in proper motion. It is of M1-M2 stellar type. Its trajectory on the sky locates it at the center of the SNR, 6,000–8,000 years ago, a unique characteristic among the the sample. Spectra allow a stellar parameters determination and a chemical abundance analysis. In conclusion, we have a candidate to be the surviving companion of the SN Ia that resulted in SNR G272.2-3.2. It is supported by its kinematical characteristics and its

trajectory within the SNR. This opens the possibility of a single-degenerate scenario for a SN Ia with an M-type dwarf companion.

Keywords: Supernovae, general; supernovae, Type Ia; *Gaia* EDR3

1. INTRODUCTION

Type Ia supernovae (SNe Ia) are powerful calibrated candles, whose use as distance indicators in cosmology led to the discovery of the accelerated expansion of the universe (Riess et al. 1998; Perlmutter et al. 1999), and currently are major tools in the exploration of the nature of dark energy (Rose et al. 2020; Hayden et al. 2021). Besides, SNe Ia are the main producers of the Fe-peak elements in the universe (see, for instance, Branch & Wheeler 2017).

However, there is still a lack of knowledge concerning the exact nature of the progenitors of the SNe Ia: on their explosion mechanism and on the kind of stellar systems from which they arise, both points being closely related. There is now a universal agreement that they are produced by the thermonuclear explosion of a white dwarf made of carbon and oxygen (a C+O WD), with a mass not far from the Chandrasekhar mass. But the explosion might be initiated close to the center of the star, when the mass reaches the Chandrasekhar limit due to accretion of material from a close binary companion (Whelan & Iben 1973), or result from compression produced by the detonation of a helium layer close to the surface of the WD (Livne 1990; Livne & Arnett 1995) or by the collision with another WD (Rosswog et al. 2009). In the last two cases, the exploding WD would have a mass below the Chandrasekhar mass. The WD progenitor of the SN Ia must be in a close binary system in all cases. The companion, the mass donor, may either be a star in any stage of thermonuclear burning (Whelan & Iben 1973; Nomoto 1982), that being called the single-degenerate (SD) scenario, or be another WD (Webbink 1984; Iben & Tutukov 1984): the double-degenerate (DD) scenario. The core-degenerate (CD) model of SN Ia explosion (Kashi & Soker 2011; Soker 2013), in which a WD merges with the electron-degenerate core of an asymptotic giant-branch (AGB) star can be included within the DD scenario. It is unknown what fraction of the observed SNe Ia corresponds to each of the two scenarios. In the DD channel, in most cases considered, both WDs should be destroyed by the explosion, no bound remnant being left. There is a possible exception, though, in the case of explosions triggered by the detonation of a surface layer made of He, accreted by the exploding WD from a less massive WD companion: then, the outburst might happen when the mass-donor has not yet been tidally disrupted. Due to its very high orbital velocity, the WD companion should be ejected as a *hypervelocity star* ($v > 1,000 \text{ km s}^{-1}$). This happens in the *dynamically driven double-degenerate, double-detonation* scenario, D⁶ (Shen & Moore 2014; Shen & Schwab 2017; Shen et al. 2018).

In the SD case, the binary companion of the exploding WD survives (Marietta et al. 2000; Pakmor et al. 2008; Pan et al. 2012a,b). The surviving companion might be in any evolutionary stage: main sequence, subgiant or red giant, be a helium or a sdB star (see Wang & Han 2012; Maoz et al. 2014; Ruiz-Lapuente 2014, 2019, for reviews). Of course, the detection of such companions at the location of a SN Ia would confirm the SD scenario (for that particular SN at least and thus for some fraction of them).

In the hydrodynamical simulations of the impact of the SN Ia ejecta with the companion, different kinds of stars have been considered: main-sequence (MS) stars (Marietta et al. 2000; Pakmor et al. 2000; Pan et al. 2012a; McCutcheon et al. 2022), subgiants (SG) (Marietta et al. 2000; Pan et al. 2012a), helium stars (Pan et al. 2012a; Liu et al. 2013a), red-giant (RG) stars (Marietta et al. 2000; Pan et al. 2012a), and sdB stars (Bauer et al. 2019). These calculations predict the state of the companion just after the SN Ia explosion. Different amounts of mass have been stripped by the impact with the ejecta and the stars are bloated and overheated. Those results provide the initial conditions to calculate the subsequent evolution of the companion stars.

The time evolution of possible SN Ia companions, on scales from hundreds to thousands of years, has been calculated by Podsiadlowski (2003), for a SG companion, Pan et al. (2012b, 2014), Shappee et al. (2013) and Rau & Pan (2022), for MS and SG companions, by Pan et al. (2012b, 2014) for RGs, by Bauer et al. (2019) for sdB stars, and by Liu et al. (2022) for He stars. The calculations predict the changes in luminosity and effective temperature of the stars, starting from the time they recover hydrostatic equilibrium after experiencing the impact of the SN ejecta. The stars are then overluminous as compared with their previous state and they evolve, on thermal time scales, to meet the characteristics corresponding to the new mass and thermonuclear burning stage. Pan et al. (2014) have also calculated the chemical pollution of the atmospheres by the ejecta.

One effect due to the star having been in a close binary system previous to the explosion are high space velocities (due to their orbital velocities prior to the disruption of the binary, in addition to the kick imparted by the ejecta)¹. Therefore, when searching for possible companions within the remnants of recent SNe Ia, one should look for high spatial velocities, paying attention to the past trajectories, and also for anomalous positions in the color-magnitude and color-color diagrams of the stars close to the center of the SNR. We should also look for possible chemical enrichment, in Fe-peak elements namely. Given the current observational means, only remnants of SNe Ia that took place in our Galaxy or in the Large Magellanic Cloud (LMC) have been explored in search for surviving companions, at present.

¹ Companions that orbit at large separations from the exploding white dwarf would have lower space velocities when the system is disrupted. Some red giants companions would have low peculiar velocities, but those surviving stars would be too luminous companions (Marietta, Burrows & Fryxell 2000) and have not been seen in the SN Ia remnants explored so far.

Up to 14 supernova remnants (SNRs) of the Ia type have been identified in the Galaxy and 12 in the LMC (Ruiz-Lapuente 2019). Of the former, only three have been explored (corresponding to the “historical” SNe Ia). They are those of SN 1572, or Tycho Brahe’s SN (Ruiz-Lapuente et al. 2004, 2019; González Hernández et al. 2009; Kerzendorf et al. 2009, 2013, 2018a; Bedin et al. 2014), of SN 1604, or Kepler’s SN (Kerzendorf et al. 2014; Ruiz-Lapuente et al. 2018), and of SN 1006 (González Hernández et al. 2012; Kerzendorf et al. 2012, 2018b; Shields et al. 2022). No indisputable companion candidate has been found in any of them. In the case of SN 1006, the absence of candidates points to a DD origin of the SN. In that of SN 1604 the same absence, joined to the characteristics of the SNR suggested the CD scenario (Ruiz-Lapuente et al. 2018). A candidate has been found for SN 1572, but the identification is in dispute (see the references above).

Five SNRs of the Ia type have been explored in the LMC: SNR 0509–67.5 (Schaefer & Pagnotta 2012; Litke et al. 2017), SNR 0519–69.0 (Edwards et al. 2012; Li et al. 2019), SNR N103B (Li et al. 2017), SNR 0505–67.9 (DEML71), and SNR 0548–70.4 (Li et al. 2019). No clear surviving companion candidate has been found in any of them but a star in N103B has characteristics compatible with being a surviving SG (Li et al. 2017), and two other stars, in 0519–69.0 and DEML71 respectively, have large radial velocities and they might also be SN companions (Li et al. 2019).

Out of the still unexplored SN Ia Galactic SNRs, most are at large distances and located close to the Galactic plane, which causes them to be very heavily reddened. That is not the case, however, of SNR G272.2–3.2, at a distance $\sim 1\text{--}3$ kpc. The EDR3 of *Gaia* now provides the parallaxes, proper motions and photometry allowing a first exploration of the central region of this SNR. Knowledge of the parallaxes allows to select the stars, close to the center of the SNR, which are at distances compatible with that of the remnant. We look for peculiar proper motions and compare the HR diagram of the sampled stars with the evolutionary paths predicted for different types of surviving companions. That already allows us to exclude the presence of several kinds of proposed candidates and to select stars deserving further analysis.

In the next Section we summarize the characteristics of the SNR G272.2–3.2 and we define the search area for the possible companion star. Observations are described in Section 3. Proper motions, their transformation to tangential velocities and a kinematic outlier are treated in Section 4. Reddening of the observed field is discussed together with the stellar spectra obtained, in Section 5. The stellar parameters of our unique peculiar star are determined and a chemical analysis is done in Section 6. In Section 7, the characteristics of this star are further discussed. Color–magnitude and the HR diagrams, along with their comparison with the evolutionary tracks predicted for different types of companions are dealt with in Section 8. Exploration of more extended areas than in Section 2 and search for the possible presence of hypervelocity stars are examined in Section 9. All results are summarized and conclusions drawn in the final Section.

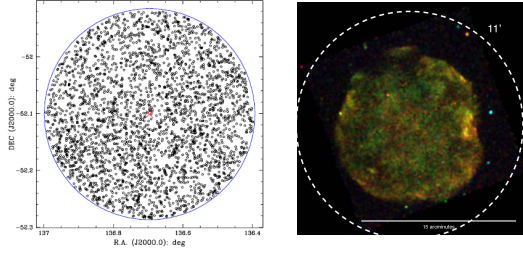


Figure 1. Left panel: positions of the 3,082 stars in our sample. The red cross marks the centroid of the G272.2-3.2 SNR, and the blue circle corresponds to the 11 arcmin radius around it. Right panel: the 11 arcmin radius circle superimposed to an X-ray image of the SNR.

2. G272.2-3.2

The SNR G272.2-3.2 was discovered in X-rays by Greiner & Egger (1993) during the *ROSAT All Sky Survey*, details being given in Greiner, Egger & Aschenbach (1994). Radio observations by Duncan et al. (1997) measured a diameter ~ 15 arcmin for the remnant. It has later been studied, in X-rays, by Harrus et al. (2001), Lopez et al. (2011), McEntaffer et al. (2013), Yamaguchi et al. (2014) and Kmitsukasa et al. (2016), with mounting evidence, from the measurement of overabundances of Ar, Ca, Si, S, Fe and Ni, that it was produced in a SNIa.

Chandra observations have provided measurements of chemical abundance ratios that are in good agreement with the predictions for delayed detonation models of SN Ia explosions (Sezer & Gök 2012).

The SNR is at a distance $d = 1.8_{-0.8}^{+1.4}$ kpc (Greiner et al 1994) or $d \sim 2 - 2.5$ kpc (Harrus et al. 2001; Kamitsukasa et al. 2016). Its age is estimated to be $7,500_{-3300}^{+3800}$ yr (Leahy et al. 2020; Xiang & Jiang 2021).

It is located about 110 pc below the Galactic plane. The radius of the remnant is about 8 arcmin, and its centroid lies at $\alpha_{J200} = 09^h 06^m 45^s.7$, $\delta_{J2000} = -52^\circ 07' 03''$ (Greiner & Egger 1993), which corresponds to the Galactic coordinates $l = 272^\circ 12' 36.9''$, $b = -3^\circ 10' 34.4''$.

We have searched in the *Gaia* EDR3 database for the stars within a radius of 11 arcminutes (thus extending beyond the whole SNR), and with parallaxes corresponding to distances $1 \text{ kpc} \leq d \leq 3 \text{ kpc}$. That has produced a sample of 3,082 stars (see Figure 1). The 11 arcmin radius is slightly above the arc described by a star moving at 500 km s^{-1} , perpendicularly to the line of sight and a distance of 2 kpc, in 12,000 yr. Wider search radii are considered and the corresponding results presented and discussed in Section 9.

Besides parallaxes and proper motions, we have also extracted the *Gaia* photometry of the stars in our sample (left panel of Figure 2). The photometry in Figure 2 is still uncorrected for interstellar extinction and reddening.

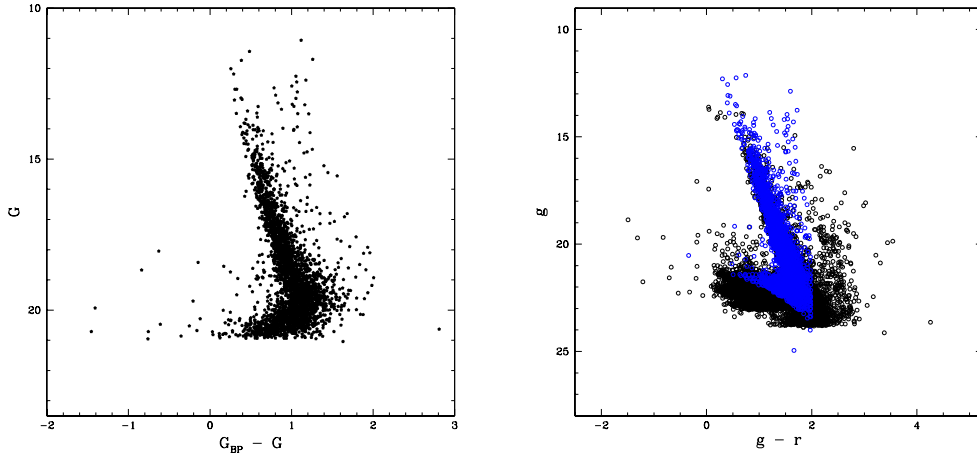


Figure 2. Left: The G vs $G_{BP} - G$ diagram for the stars in our sample, uncorrected from reddening and extinction. Right: A g vs $g - r$ diagram showing the stars of our sample (in blue) superimposed to those obtained from the *DECaPS* survey (in black), within the same cone but with no limitation on distances (which are unknown there). We see the consistency between the *Gaia* EDR3 photometry and that of the *DECaPS* survey (see main text). The *Gaia* magnitudes have been transformed into the *SDSS* magnitudes using the expressions given by Carrasco (*Gaia Data Release Documentation* 5.3.7). Errors of up to 0.16 mag can be made when transforming G into g magnitudes.

3. OBSERVATIONS

3.1. *Gaia* EDR3

As stated above, the *Gaia* EDR3 has been used to obtain the proper motions, parallaxes and photometry in the G , G_{BP} and G_{RP} bands, for the stars within a circle of 11 arcmin radius on the sky, around the centroid of SNR G272.2–3.2, and parallaxes corresponding to distances in the selected range.

Gaia EDR3, released on December 2020, contains the full astrometric solution (positions, parallaxes and proper motions) for around 1.468×10^9 stars, with a limiting magnitude $G \sim 21$ mag.

It also gives G magnitudes for 1.806×10^9 sources, and G_{BP} and G_{RP} for around 1.542×10^9 and 1.555×10^9 sources, respectively. It is publicly available².

3.2. *DECaPS*

We have also used the photometric data from *DECaPS* (*DECam Plane Survey*). This is a five-band optical and infrared survey of the southern Galactic plane with the *Dark Energy Camera* (*DECam*) at Cerro Tololo. It covers about 1,000 square degrees (the low latitude Galactic plane south of $\delta < 30^\circ$).

The survey, which is publicly available³, has a depth of 23.7, 22.8, 22.2, 21.8 and 21.0 mag in the *grizY* bands. We have explored the same circle of 11 arcmin radius around the centroid of G272.2–3.2 as in *Gaia* EDR3, but with no limits on distance here (parallaxes unknown). That has yielded 38,019 stars with complete *gri* photometry at least. Our *Gaia* DR3 sample sits at the core of this more extended sample, which shows the consistence between the two photometric systems (see the right panel of Figure 2). There, *Gaia* magnitudes have been transformed into the *SDSS* magnitudes using the expressions given by Carrasco (*Gaia Data Release Documentation* 5.3.7). An error by up to 0.16 mag can be made when going from G to g magnitudes).

3.3. *Spectra*

Several stars have been observed using the camera on the *Goodman* spectrograph (Clemens et al. 2004), mounted on the 4.1m *SOAR* telescope. The 600 lines mm^{-1} grating and the 1.0 arcsec slit have been used, providing a resolution of $\sim 4.3 \text{ \AA}$ or better ($R \sim 1,400$) and covering from 4,550 \AA to 7,050 \AA . We reduced the *Goodman* data following usual steps, including bias subtraction, flat-fielding, cosmic ray rejection using *LA-Cosmic* (van Dokkum 2001), wavelength calibration, flux calibration, and telluric correction using our own custom *IRAF* routines. The telluric correction was performed using a flux standard observed at the beginning of the night with the same configuration of our science targets. A final combined spectrum was obtained by combining the individual spectra, weighted by the signal-to-noise ratio.

Spectra of the same stars have also been obtained with the *MIKE* spectrograph⁴ at the 6.5m *Clay* telescope. *MIKE* is a high-resolution optical spectrograph with a wavelength coverage from 3,500 to 9,500 \AA . The stars have been observed several nights (see Table 1). We used the Red arm, covering the wavelength range 4,000–9,500 \AA , with a slit width of 0.7 arcsec and a binning of 2×2 providing a resolving power of $R \sim 28,000$ (equivalent to a FWHM $\sim 10.7 \text{ km s}^{-1}$ and a pixel size of 0.069 \AA (equal to 2.69 km s^{-1}).

The *CarPy* pipeline (Kelson et al. 2000; Kelson 2003) has been used to reduce each single night separately. The final product was a sky-subtracted and wavelength-calibrated spectrum for each separate order per night. A spectrophotometric standard

² gea.esac.esa.int/archive/

³ <http://decaps.skymaps.info>

⁴ Bernstein, R., Shethman, S.A., Gunnels, S.M., et al. SPIE, 4841, doi:0.117/12.461502

Table 1. Summary of Spectroscopic Observations

<i>SOAR</i> telescope/ <i>Goodman</i> spectrograph				
Date	Source	exp.time	slit	airmass
Feb07	<i>Gaia</i> EDR3 5323900211541075328	2hr	1.0	1.20
Mar10	<i>Gaia</i> EDR3 5323871314998012928	1hr45min	1.0	1.10
Apr26	<i>Gaia</i> EDR3 5323852210990643584	1h45min	1.0	1.20
<i>Clay</i> telescope/ <i>MIKE</i> spectrograph				
Nov20	<i>Gaia</i> EDR3 5323900211541075328	1hr	0.70	1.20
Nov21	<i>Gaia</i> EDR3 5323900211541075328	1hr20min	0.70	1.15
Feb25	<i>Gaia</i> EDR3 5323900211541075328	1hr20min	0.70	1.12
May19	<i>Gaia</i> EDR3 5323900211541075328	2hr	0.70	1.23
May21	<i>Gaia</i> EDR3 5323871314998012928	2hr	0.70	1.23

star has also been observed each night in order to perform relative flux calibration. This was done using *IRAF* routines (*standard*, *sensfunc* and *calibrate*), resulting in a spectrum calibrated to the correct flux scale and corrected for extinction. In order to obtain the final stacked spectrum, the flux-calibrated spectrum for each order in each night has been combined using the *IRAF* task *scombine*. This led to an 1D spectrum over the full wavelength range.

4. SPACE VELOCITIES.

Peculiar space velocities as compared with those of the surrounding stars are among the likely characteristics of surviving companions of SNe Ia explosions. In Figure 3 we show the distribution of proper motions in right ascension, RA (left) and in declination, DEC (right). The mean proper motion in RA (μ_α^*) is -4.8 mas/yr, with a standard deviation $\sigma = 3.12$ mas/yr, while in DEC (μ_δ) we have a mean of 4.44 mas/yr with $\sigma = 3.11$ mas/yr. There is a star, *Gaia* EDR3 5323900211541075328 (MV-G272) (RA = $09^h 06^m 24.66^s$; DEC = $-52^\circ 03' 09.684''$, $G = 19.854$ mag) with $\mu_\alpha^* = -22.80$ mas/yr and $\mu_\delta = 30.60$ mas/yr, which is the only extreme outlier in the two proper motion distributions: at 5.8σ from the mean in RA proper motion and at 8.4σ in DEC.

The distribution of total proper motions ($\mu = \sqrt{(\mu_\alpha^*)^2 + (\mu_\delta)^2}$) is shown in Figure 4 (left panel). Since we know the distances to the stars, we can calculate their total velocities perpendicularly to the line of sight, v_{tan} (using the expression: $v_{tan} = 4.7485 \times \mu/\varpi$, ϖ being the parallax). The resulting distribution is shown in the right panel of Figure 4. Here we see again the same outlier, with a total proper motion of 38.15 mas/yr (that is 8.9σ above the mean). The distance to the star, from its parallax, is $d = 1.32_{-0.39}^{+1.00}$ kpc, which gives a tangential velocity $v_{tan} = 239_{-70}^{+181}$ km s⁻¹ (5.4σ above the mean).

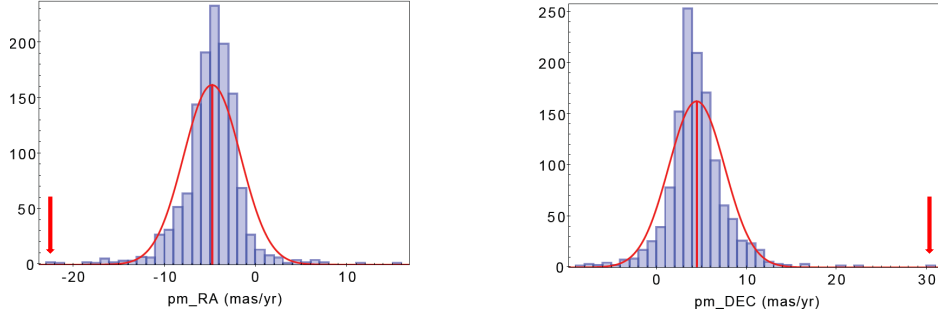


Figure 3. Left: histogram of the distribution of proper motions in RA of the stars in our sample. Right: same, for the proper motions in DEC. The Gaussian fits are overplotted in red.

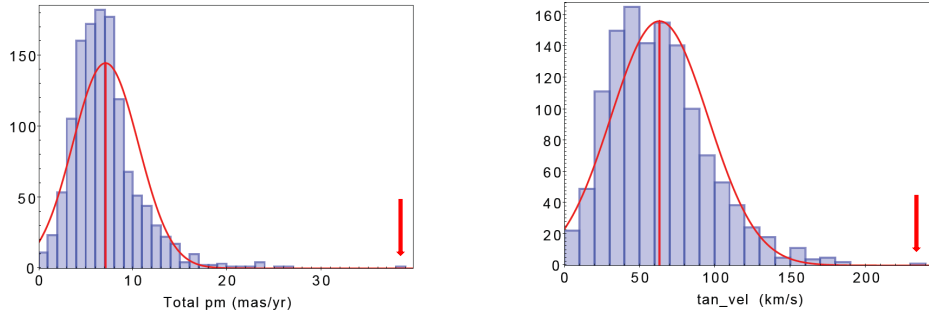


Figure 4. Left: histogram of the distribution of the total proper motions of the sampled stars. Right: same for the velocities v_{tan} , perpendicular to the line of sight.

Total speeds of that order are expected for MS or SG companions of a SN Ia (Han 2008; see also Table 1 in Pan et al. 2014), so this star deserves further study.

Since the SNR G272.2-3.2 has a minimum age of $\sim 4,500$ yr, any possible surviving companion should have travelled an appreciable distance from the site of the explosion, by now. From the proper motions measured, we can infer its position at the time of the SN outburst. In Figure 5, that is made for an age of 8,000 yr. We see that star MV-G272, located at the periphery of the SNR at present, was very close to the center by then.

The *Gaia* EDR3 does not provide information on the radial velocities v_r of any of those stars. From a spectrum of MV-G272 (see next Section), we have measured a barycentric velocity $v_{bar} = 92.6 \pm 0.5 \text{ km s}^{-1}$ ($v_r = 77.3 \text{ km s}^{-1}$ in the LSR). That gives $v_{tot} = 256^{+181}_{-70} \text{ km s}^{-1}$ (barycentric), for this star.

It can be seen, from Figures 3 and 4, that there are a few stars at $\sigma > 3$ in the corresponding distributions, but in view their positions relative to the SNR and their trajectories, they are not viable candidates to be companions of the SN.

4.1. The kinematics of star *Gaia* EDR3 5323900211541075328/MV-G272

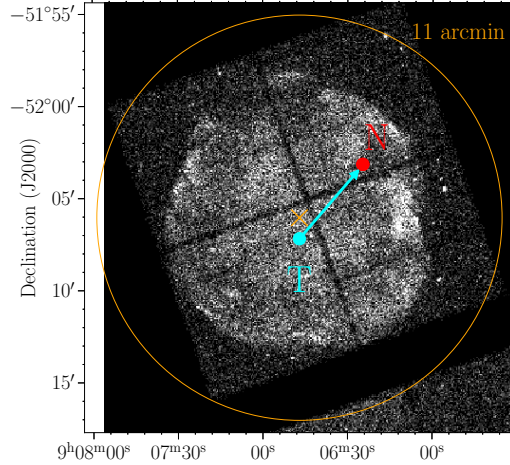


Figure 5. Present position of the fastest moving star, MV-G272 (red dot, labelled *N*), compared with that it had 8,000 yr ago (blue dot, labelled *T*). The picture has been superposed to the Chandra image of the SNR in keV range (Sánchez-Ayaso et al. 2013). We see that the star, now nearing the edge of the SNR, was close to the center (marked with a red cross), then. The errors in the proper motions being very small, the uncertainty as to the past position is not larger than the size of the plotted point.

The star MV-G272 looks like a possible candidate to be the surviving companion of the SN Ia that gave rise to SNR G272.2–3.2. Subsequently, its kinematics is analyzed in more detail below. We will look at the motion in Galactic coordinates taking for comparison the current Besançon model of the Galaxy (<https://model.obs-besancon.fr>). Since the star is a M1-M2 dwarf with solar metallicity (see next Section), we will only use, from the model, M dwarfs with the same metallicity and located at distances $1 \text{ kpc} \leq d \leq 2 \text{ kpc}$, like the candidate star. The resulting distributions in μ_l^* , μ_b and v_r of the model stars are shown in Figure 6.

With $\mu_l^* = -37.96 \text{ mas/yr}$, star MV-G272 is at 6.1σ above the mean, while its $\mu_b = 3.85 \text{ mas/yr}$ is at 1.4σ only, and $v_r = 77.1 \text{ km s}^{-1}$ in the LSR is at 2.4σ . Thus, only the motion along the Galactic plane is really peculiar as compared with the Besançon model.

We can also select the M dwarf population within our sample, equally at distances $1 \text{ kpc} \leq d \leq 2 \text{ kpc}$, and look at its distribution in μ_l and μ_b . In this way we know how star MV-G272 moves as compared with the surrounding stars of the same type. The distributions are shown in Figure 7. This star is a clear outlier in μ_l^* , at 7.4σ above the mean, while it is only at 1.7σ in μ_b ,

To investigate further the kinematics of star MV-G272, we have also calculated its orbit, using *GravPot16* (Fernández-Trincado 2017). In Figure 8 we show the 3D orbit and its projections on the XY, XZ and YZ planes of the referential system of the Galaxy. We see that the projection of the orbit on the XY plane is very eccentric, with $e = 0.447$. Only 13 stars in our sample have radial velocities determined in *Gaia* EDR3, and only them can thus be used to calculate eccentricities. The mean

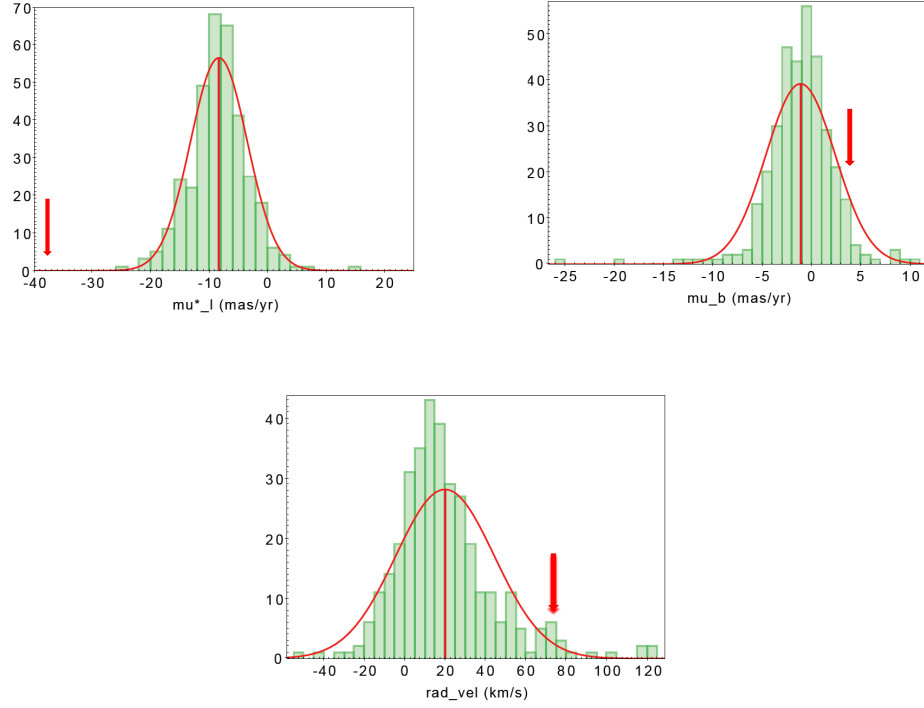


Figure 6. The distributions in μ_l^* , μ_b (two upper panels) and v_r (lower panel) of the M dwarf stars with about solar metallicity and at distances $1 \text{ kpc} \leq d \leq 2 \text{ kpc}$, in the direction of G272.2–3.2, from the Besançon model of the Galaxy (<https://model.obs-besancon.fr>; see text for details).

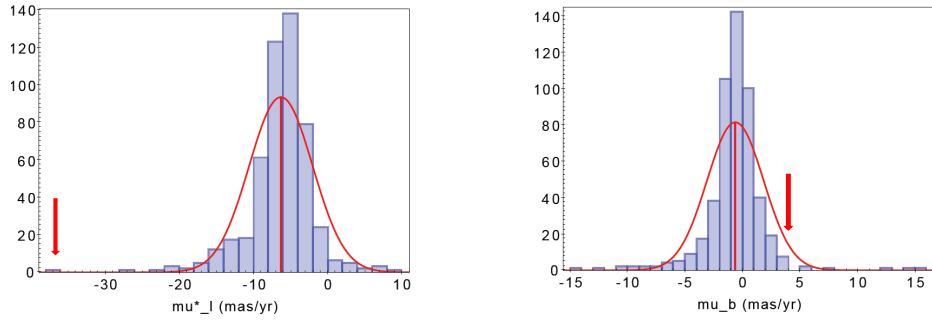


Figure 7. The distributions in μ_l^* (left panel) and μ_b (right panel) of the M dwarf stars at distances $1 \text{ kpc} \leq d \leq 2 \text{ kpc}$ in our sample from *Gaia* EDR3.

eccentricity is $\langle e \rangle = 0.167$, with $\sigma = 0.063$. Therefore, that of star MV-G272 is 4.5σ above the mean, as illustrated in Figure 9.

5. REDDENING AND SPECTROSCOPY

Measured *Gaia* magnitudes are affected by absorption due to intervening gas and dust. In order to compare the observed photometry with theoretical models of the

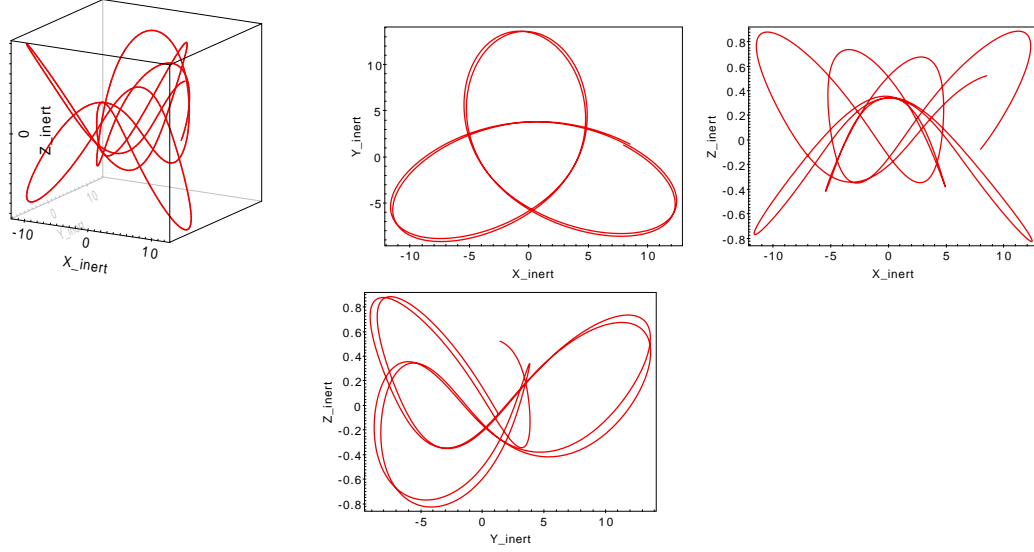


Figure 8. 3D orbit of star MV-G272 along 10^9 yr (forward in time) and its projections on the XY, XZ and YZ planes of the referential system of the Galaxy.

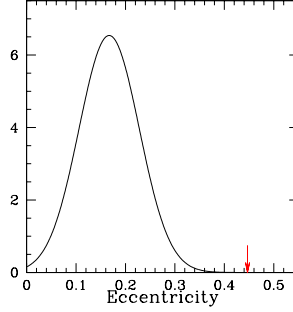


Figure 9. The eccentricity distribution of the orbits of the 13 stars in our sample having their radial velocities measured in *Gaia* EDR3. An arrow marks that of star MV-G272.

Table 2. *Gaia* EDR2 stars used for the reddening estimate

<i>Gaia</i> ID	G	G_{BP}	G_{RP}	T_{eff}	$\log g$	[Fe/H]
5323849427851815808	12.26	13.31	11.25	5000	3	0
5323897355382648960	12.65	13.43	11.77	5000	3	0
5323899352554079101	13.26	14.30	12.26	4500	3	0
5323899352554079104	13.25	14.28	12.25	4500	3	0

evolution of possible stellar companions after the SN Ia explosion, the extinction in different bands must be accurately estimated and subtracted.

There are only four stars in our sample which have their parameters T_{eff} , $\log g$ and [Fe/H] determined in the *Gaia* EDR2 (see Table 2).

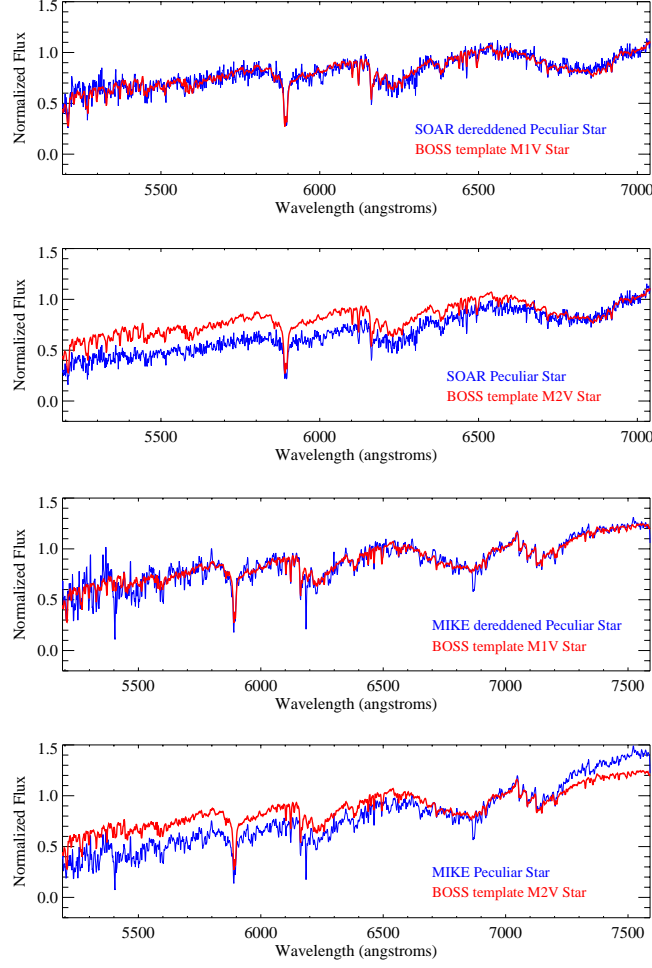


Figure 10. Two upper panels: spectrum of star *Gaia* EDR3 5323900211541075328 (MV-G272), taken with the *Goodman* spectrograph at the 4.1m *SOAR* telescope. In the first panel, it is corrected for a reddening $E(B - V) = 0.532$ and superposed to the template for a M1 dwarf with solar metallicity, while in the second one it is compared with the template for a M2 dwarf with the same metallicity but without correction for reddening there. Two lower panels: spectrum of the same star, taken with the *MIKE* spectrograph at the 6.1m *Clay* telescope, covering a similar wavelength range. In the first panel, it is superposed to the template for a M1V star with solar metallicity and corrected for a reddening $E(B - V) = 0.532$. In the second panel, it is superposed to the template for a M2V star, also with solar metallicity, without correcting for reddening. Observed and template spectra have been normalized by dividing by a constant equal to the mean value of the fluxes in the spectral range 6,950-7,000 Å. The *MIKE* spectrum has been degraded to a resolution $R \sim 2,000$, analogous to that of the *BOSS* templates used by the *PyHammer* code. All spectra have been sampled with a pixel size of 1.298 Å per pixel.

Using the expressions by Carrasco⁵, we translate their magnitudes to the Johnson’s UBVRI system and then compare the measured colors with those corresponding to stars with the same parameters (Hundaselt et al. 2000). From the color excesses, we deduce the extinctions A_V , A_R , A_I for each of the four stars. Since the stellar

⁵ *Gaia Data Release Documentation* 5.3.7; see also Jordi et al. (2010)

parameters from *Gaia* EDR2 do not seem very accurate, we do not expect a perfect coincidence in the values obtained for the different stars, but the average value for A_V is 1.65 mag, in agreement with that obtained from the spectral fits below.

Another estimate comes from fitting spectra of star MV-G272, taken with the *MIKE* spectrograph at the 6.5m *Clay* telescope and with the *Goodman* spectrograph at the 4.1m *SOAR* telescope (both covering similar wavelength ranges). We have used the *PyHammer* tool (Kesseli et al. 2017, 2020) to infer that the best fit spectral type is M1V-M2V. This code uses a set of templates for different spectral types and luminosity classes with a discrete set of metallicity values with a step of ~ 0.5 dex, created from observed SDSS/BOSS spectra at $R \sim 2,000$. In Figure 10 are shown the fits of both spectra to the template for a M1V star, with solar metallicity and a reddening of $E(B-V) = 0.532$ (two top panels), and to a M2V star, with negligible reddening and solar metallicity too (bottom panels). Good fits to a M1V spectrum can also be obtained for smaller reddening and a somewhat higher metallicity ($[\text{Fe}/\text{H}] = +0.5$). We prefer the first fits, which correspond, for $A_V = 3.1 \times E(B-V)$, to $A_V = 1.65$ mag, and coincides with the estimate made from photometry.

As mentioned above, we have measured a radial velocity of $v_r = 92.6 \pm 0.5$ km s $^{-1}$ (barycentric) or $v_r = 77.3 \pm 0.5$ km s $^{-1}$ (LSR), using the *MIKE* spectrum.

A deeper and more complete analysis of the *MIKE* spectrum is made in the next Section.

6. STELLAR PARAMETERS AND METALLICITY OF *GAIA* EDR3 5323900211541075328 (STAR MV-G272)

We have analysed the high-resolution *MIKE* spectrum ($R \sim 28,000$) to try to estimate global metallicity and some element abundances, from individual lines available in the red part of the *MIKE* (Bernstein et al. 2003) spectrum. The star is quite faint, which gives an estimated S/N ~ 18 at 7,500 Å. The spectrum has a total exposure time of 13,200 s. For comparison we also analysed two high-resolution CARMENES VIS spectra (Reiners et al. 2018) of two stars classified as M1V stars and the solar ATLAS spectrum (Kurucz et al. 1984) as a reference (see Appendix and discussion below). The two CARMENES spectra of these stars have been recently analysed (Marfil et al. 2021) with the SteParSyn code (Tabernero et al. 2022, 2021), providing the following set of parameters: $T_{\text{eff}}/\log g/[\text{Fe}/\text{H}] = 3,603/4.99/-0.52$ for star Karmn J00183+440 (GX And) and $T_{\text{eff}}/\log g/[\text{Fe}/\text{H}] = 3,825/4.94/-0.04$ for star Karmn J05415+534 (HD 233153). Deriving the metallicities of M dwarfs even with high quality spectra at high resolution is a challenging exercise, with differences of 0.3 dex from different methods (Passeger et al. 2022). These analyses have been done from individually resolved lines at very high resolution of these very high quality spectra, using those codes mentioned above.

We have also analysed single CARMENES VIS spectra of these two stars and the solar ATLAS spectrum, all degraded to a resolving power of 28,000 and with injected

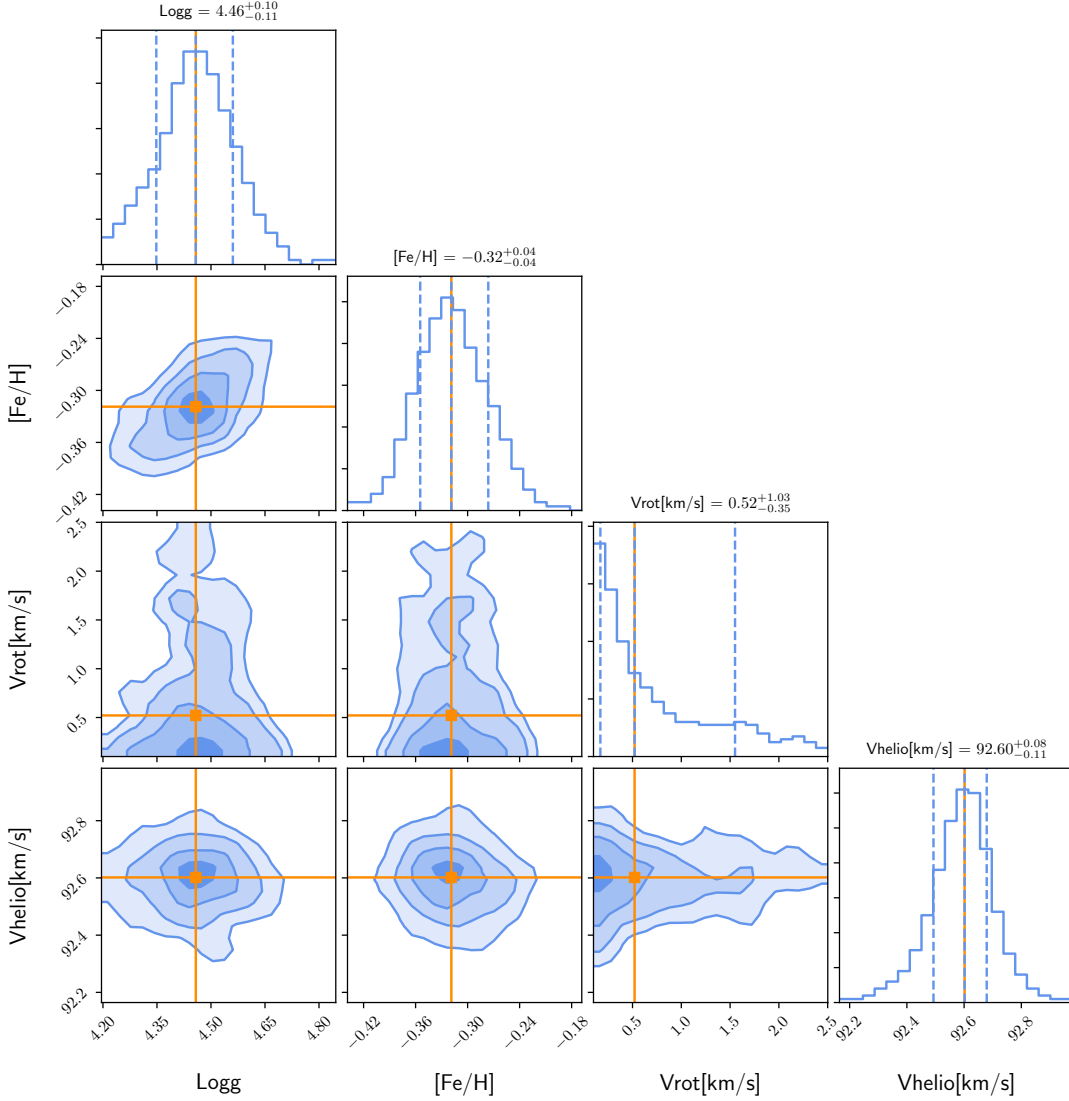


Figure 11. Posterior distributions of the parameters of the analysis of the *MIKE* spectrum using our Bayesian code to derive the effective temperature T_{eff} , surface gravity $\log g$, metallicity $[\text{Fe}/\text{H}]$, rotational velocity V_{rot} , and heliocentric radial velocity V_{helio} . A fixed T_{eff} of about 3800 K has been assumed here.

noise to $S/N \sim 18$ at $7,500 \text{ \AA}$, to match the *MIKE* spectrum resolution and quality. Thus, we implemented a Bayesian Python code that compares the observed spectrum with a synthetic spectrum in the spectral range $7,000\text{--}8,750 \text{ \AA}$. Both the observed spectra and the synthetic spectra are normalized using a running mean filter with a width of 200 pixels at a dispersion of 0.069 \AA per pixel (see Figures in Appendix). We performed a Markov Chain Monte Carlo (MCMC) with 5,000 chains implemented in EMCEE (see Foreman-Mackey et al. 2013), sufficient to get a statistically significant result. We use a small $3 \times 3 \times 3$ grid of synthetic spectra with values $T_{\text{eff}}/\log g/[\text{Fe}/\text{H}]$ of $3500\text{--}4500/3.0\text{--}5.0/-1.0\text{--}0.5$ and steps of $250 \text{ K} / 0.5 \text{ dex} / 0.5 \text{ dex}$, computed with

the SYNPLE⁶ code, assuming a microturbulence $\xi_{\text{mic}} = 0.8 \text{ km s}^{-1}$, and ATLAS9 model atmospheres with solar α -element abundances ($[\alpha/\text{Fe}] = 0$, see Castelli & Kurucz 2003). Details of the fits are shown in the Appendix.

The model includes as free parameters, the effective temperature, T_{eff} , surface gravity, $\log g$, $[\text{Fe}/\text{H}]$, rotational velocity, V_{rot} , and relative radial velocity, V_{rel} (Figure 11). We run a simulation leaving free all the parameters and found that the simulation converges to a T_{eff} value at the lower edge of the grid. A similar result with a lower T_{eff} value by about 250K than those obtained at high-resolution was obtained when analysing the two CARMENES spectra. Thus we decided to run a simulation by fixing the T_{eff} at 3800 K for our target star. The posterior distributions of the simulation is displayed in Figure 11, that provide the values $\log g/[\text{Fe}/\text{H}] = 4.46/-0.32$. For the two degraded CARMENES spectra we got $T_{\text{eff}}/\log g/[\text{Fe}/\text{H}] = 3,580/4.37/-0.69$ for star Karmn J00183+440 (GX And) and $T_{\text{eff}}/\log g/[\text{Fe}/\text{H}] = 3,805/4.67/-0.04$ for star Karmn J05415+534 (HD 233153). As seen in Figure 12, the rotational velocity is not resolved with the instrumental full width at half maximum FWHM of 10.7 km s^{-1} , providing a value consistent with zero and an upper-limit at 3σ of $V_{\text{rot}} < 3 \text{ km s}^{-1}$. The heliocentric radial velocity of the star is estimated at $92.60 \pm 0.5 \text{ km s}^{-1}$, which translates into $V_{\text{LSR}} = 77.3 \pm 0.5 \text{ km s}^{-1}$ in the LSR.

We analysed the solar ATLAS spectra to get the reference solar element abundances, including all the relatively isolated features available in the *MIKE* spectrum of our target star, including five Fe lines, seven Ti lines, two Cr and Na lines and one Ni and Al lines. For that exercise we used a grid of models with values $T_{\text{eff}}/\log g/[\text{Fe}/\text{H}]$ of $5,500 - 6,000/4.0 - 5.0/-0.5 - 0.5$ and steps of $250 \text{ K} / 0.5 \text{ dex} / 0.5 \text{ dex}$, assuming a fixed $\xi_{\text{mic}} = 0.95 \text{ km s}^{-1}$. The analysis of the degraded solar spectrum provided all the element abundances within $[\text{X}/\text{H}] = -0.13$ for Ti and -0.03 dex for Na. The Ca features were discarded because they provided very different results for Ca I and Ca II lines even in the solar case. The tentative abundance ratios found in the target star are $[\text{Na}/\text{H}] = -0.10$, $[\text{Al}/\text{H}] = -0.23$, $[\text{Ti}/\text{H}] = -0.05$, $[\text{Cr}/\text{H}] = -0.08$, and $[\text{Ni}/\text{H}] = -0.23$. These values may indicate a slight enhancement at $0.1-0.2 \text{ dex}$ in all the element abundances with respect to the metallicity value of $[\text{Fe}/\text{H}] = -0.32$. We consider them very tentative with this methodology in M dwarfs given also the S/N of the *MIKE* spectrum. In any case, these stars being almost fully convective, any captured material from the SN ejecta should be strongly diluted.

The characteristics of star MV-G272 are summarized in Table 3.

7. STAR *GAIA* EDR3 5323900211541075328/MV-G272 AS A POSSIBLE SNIA COMPANION

We know that, at present, star MV-G272 has the characteristics of a M1-M2 dwarf. Assuming that it were the companion of the SNIa that gave rise to the SNR G272.2-3.2 and that its mass and radius was similar to the present ones, at the time of the

⁶ Available at <https://github.com/callendeprieto/synple>

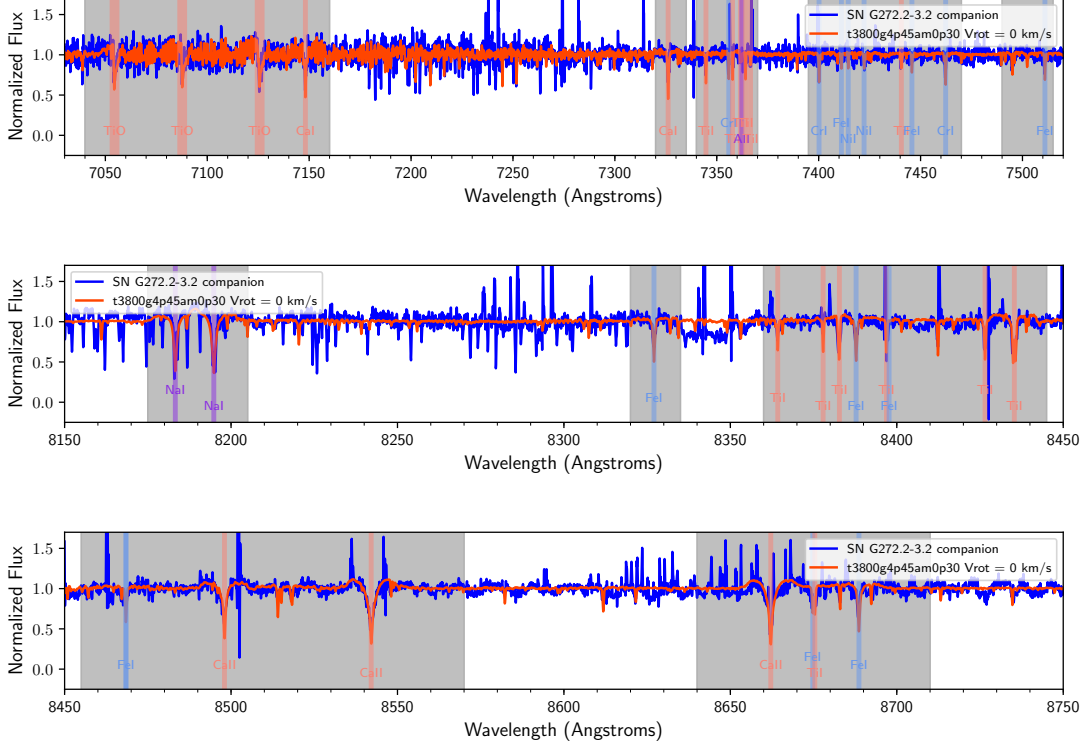


Figure 12. Normalized *MIKE* 1D spectrum of star Gaia EDR3 5323900211541075328 (MV-G272), corrected for barycentric radial velocity, and normalized to unity using a running mean filter with a width of 200 pixels at 0.069 Å per pixel, with a signal-to-noise ratio of ~ 18 at 7,500 Å. We also display an interpolated SYNPLE synthetic spectrum with the stellar parameters $T_{\text{eff}} = 3,800$ K, $\log g = 4.45$ and and metallicity $[\text{Fe}/\text{H}] = -0.3$. The regions used to estimate the metallicity are shown in grey and the different lines used for chemical analysis are also highlighted.

explosion, then it should have been in close orbit with a $1.4 M_{\odot}$ WD and filling its Roche lobe. We can calculate at which velocity should it have been ejected.

We would have, for the orbital motion of the star around the center of mass of the binary:

$$v_{\text{orb}}^2 = \frac{GM_{\text{WD}}}{a(1+q)} \quad (1)$$

where a is the orbital separation and $q \equiv M_{\text{comp}}/M_{\text{WD}}$. In our case we have $M_{\text{WD}} = 1.4M_{\odot}$ and $M_{\text{comp}} = 0.44M_{\odot}$, corresponding to a M1 dwarf (Pecault & Mamajek 2013). So, in our case, $q = 0.314$. The radius of a M1 dwarf is $R_M = 0.446R_{\odot}$ (same source).

We have, on the other hand, the Eggleton (1983) approximate formula for the Roche lobe radius R_L of the secondary star in a binary:

$$R_L = a \left[\frac{0.49}{0.6q^{-2/3} + \ln(1+q^{1/3})} \right] \quad (2)$$

Table 3. Characteristics of star *Gaia* EDR3 5323900211541075328 (MV-G272)

μ_α^* (mas/yr)	...	-22.79
μ_δ (mas/yr)	...	30.60
μ (mas/yr)	...	38.15
μ_l^* (mas/yr)	...	-37.96
μ_b (mas/yr)	...	3.85
d (kpc)	...	$1.32^{+1.00}_{-0.39}$
v_{tan} (km s ⁻¹)	...	239^{+181}_{-70}
v_r (km s ⁻¹)	...	77.3 ± 0.5 (LSR)
v_r (km s ⁻¹)	...	92.6 ± 0.5 (barycentric)
v_{tot} (km s ⁻¹)	...	256^{+181}_{-70}
G mag	...	19.85
G_{BP} mag	...	21.03
G_{RP} mag	...	18.77
Spectral type	...	M1-M2
Luminosity class	...	V
$[Fe/H]$...	-0.32 ± 0.04
M (M_\odot)	...	0.44-0.50
R (R_\odot)	...	0.446-0.482
T_{eff} (K)	...	3,600-3,850
$\log g$...	$4.46^{+0.10}_{-0.11}$
$\log(L/L_\odot)$...	-1.54/-1.39

We thus have for the orbital velocity, by making $R_L = R_M$ in (2) to obtain a and substituting it in (1):

$$v_{\text{orbit}}^2 = \frac{0.49 GM_{WD}}{R_M(1+q)[0.6q^{-2/3} + \ln(1+q^{1/3})]} \quad (3)$$

and then, rounding to unity, $v_{\text{orbit}} = 350 \text{ km s}^{-1}$. We have measured a total velocity $v_{\text{tot}} = 256^{+181}_{-70} \text{ km s}^{-1}$ for star MV-G272 (vector sum of tangential and radial velocities).

The orbital velocity is just an upper limit to the actual one before explosion, since some mass should have been stripped by the impact of the SN ejecta and the pre-explosion radius and orbital separation should also have been larger, then.

Concerning the rotational velocity, even before explosion rotation might have been slowed down due to angular momentum loss from the mass transfer to the WD. The collision with the ejecta of the SN can drastically reduce the rotational velocity. This has been shown by Liu et al. (2013b) and Pan et al. (2014). In the 3D hydrodynamical simulations of Liu et al. (2013b), the rotational velocity of the companion is reduced to only 14% to 32% of its pre-explosion value. Similar results are quoted by Pan et al. (2014), with references to their previous work (Pan et al. 2012b, 2013). An extra mechanism to slow down the rotation of the companion star after the impact of the SN ejecta would act during the evaporation phase of the surface layers of the star

(those that have not been ablated by the impact but have absorbed enough energy to become unbound). If the wind remains tied to the surface of the star by the magnetic field and is only lost at significant distances above the surface, it will carry a lot of angular momentum, thus significantly reducing the rotational velocity, (this idea is being explored by X. Meng et al. 2023, in preparation).

Finally, it must be remembered that what is actually measured is $v_{rot} \sin i$, where i is the angle made by the rotation axis with the line of sight.

Pan et al. (2012a) have calculated the amount of contamination by Fe and Ni of the surfaces of SNeIa companions. They obtained $\sim 10^{-5}M_{\odot}$ for MS star companions, $\sim 10^{-4}M_{\odot}$ for He star companions, and $\sim 10^{-8}M_{\odot}$ for RG companions (see also Pan et al. 2014). The observed contamination would, however, depend on the degree of dilution of the contaminants with the stellar envelope. Even in an early M dwarf, most of the mass, from the surface down to close to the central layers, is convective. We should thus expect a strong dilution of the material captured from the ejecta, and thus only moderate overabundances of Fe-peak elements.

8. HR DIAGRAMS

From the *Gaia* photometry and parallaxes, we can now construct HR diagrams for our sample of stars. They can then be compared with model predictions for different types of possible survivors from SNeIa explosions. There are only a few theoretical calculations of the evolution of SNeIa companions after being hit by the SN ejecta. Podsiadlowski (2003) modeled the evolution of a SG star of $2.1 M_{\odot}$ for up to 10,000 yr after the explosion, and later Shappee et al. (2013) did the same for a MS companion of $1 M_{\odot}$. In both cases, mass stripping from the impact was modeled as a fast wind and energy injection to the layers of the companion that remained bound was parameterized. The results, for the luminosities and effective temperatures of the companions, 10,000 yr after the explosion, very widely differ, as it can be seen by comparing Fig. 1 in Podsiadlowski (2003) with Fig. 4 in Shappee et al. (2013).

Di Stefano et al. (2011) (see also Justham 2011) have calculated the evolution of SNIa companions for the case in which there is long enough delay between the end of mass transfer and the explosion (due to the fast rotation of the WD) to allow the companion to become a second WD before the explosion takes place. Their calculations, however, stop at this point and there are no existing hydrodynamical simulations of the collision of the SN material with the WD, a prerequisite to know its state, thousands of years after the explosion.

Meng & Li (2019) (see also Meng & Luo 2021) have calculated the luminosities and colors of possible MS companions ending as subdwarf (sdB) stars at the time of the SN explosion but, again, neither the effects of the impact on them nor their subsequent evolution are included there. Bauer et al. (2019) have modelled the collision of SNIa ejecta with a sdB star and also the evolution after the impact, providing various useful observational predictions. Pan et al.(2014), on the other

hand, start from 3D hydrodynamic models of the companions after being hit by the SN ejecta and follow their evolution hydrodynamically until hydrostatic (but not thermal) equilibrium is recovered. Those 3D models are then projected into 1D models, whose subsequent evolution is calculated using the *MESA* (*Modules for Experiments in Stellar Astrophysics*) code⁷. In this way they predict the evolutionary tracks for MS companions up to 9,000 yr after being hit by the SN ejecta and those for He star companions until 1,000 yr after the explosion.

In Figure 13 we show the tracks followed by MS and He star companions with several masses and pre-explosion orbital parameters, taken from Pan et al. (2014). Model characteristics of MS companions are given in Table 4 (which reproduces part of their Table 1). The tracks are plotted on the g vs $g - r$ plane (Sloan colors), assuming a distance of 2 kpc. The positions of the sdB stars from Meng & Li (2019) are equally shown. Comparison is made with the stars in our *Gaia* sample and also with the larger sample from the *DECaPS* survey, which includes stars within a wider range of distances. Both samples are corrected for reddening (see Section 5, above).

We clearly see that no sdB stars are present in any of the two samples. As for the He star companions, although a few stars from the *DECaPS* survey lie not far from the ends of the tracks, this is consistent with the dispersion due to the lack of distance boundaries there. MS companions are not close to our *Gaia* sample, either. They will be discussed next.

Table 4. The main-sequence SN Ia companion models of Pan et al. (2014)

Model ¹		M_b (M_\odot)	R_b (R_\odot)	M_a (M_\odot)	R_a (R_\odot)	v_{linear} (km s ⁻¹)
A	...	1.88	1.25	1.64	3.87	179
B	...	1.82	1.50	1.65	4.76	179
C	...	1.82	2.63	1.56	7.61	136
D	...	1.63	1.19	1.43	3.42	188
E	...	1.59	1.42	1.44	3.91	191
F	...	1.55	1.97	1.30	4.09	143
G	...	1.17	0.79	0.93	4.45	271

¹ Subscript b indicates before and subscript a after the SNe Ia explosion.

In Figure 14 we compare, in the HR diagram $\log(L/L_\odot)$ vs $\log T_{eff}$, the evolutionary tracks for the MS models A–G in Table 4 with our *Gaia* sample.

The tracks calculated by Pan et al. (2014), as mentioned above, follow the evolution of the possible companions up to 9,000 yr after the explosion. That covers, at least in part, the estimated range of ages for the SNR. Only very few stars lie close to the ends of the evolutionary tracks A–G, and they do not display any kinematical peculiarity.

⁷ docs.mesastar.org/en/release-r22.05.1

Star MV-G272 lies quite apart from the tracks, but its mass should be $M \simeq 0.44 - 0.50 M_{\odot}$, less than half the smaller mass in Table 4 and Figures 13 and 14 (that of model G). No simulations of the impact of the SN ejecta nor calculations of the subsequent evolution are available for stars of such a small mass.

Very recently, Rau & Pan (2022) have extended the calculations of the post-impact evolution of MS companions down to $0.8 M_{\odot}$, the result depending of the ratio of the orbital separation to the radius of the star at the time of the explosion, for a fixed explosion energy. They follow the evolution up to more than 10^5 yr after the explosion. They find that, for the lowest mass considered ($0.8 M_{\odot}$), the luminosity remains constant and can be as low as $\sim 2L_{\odot}$ from shortly after the explosion until $\sim 10^3$ yr later. From this point on, the luminosity starts decreasing. A constant luminosity stage is common to all the masses studied ($0.8, 1, 1.5$ and $2 M_{\odot}$), such luminosity decreasing fast when going from the larger to the lower masses (see their Fig. 2). These new results appear consistent with an origin of star MV-G272 from the impact of SNIa ejecta on a MS companion of low mass.

The simplest hypothesis for the origin would be that MV-G272 was a more massive MS star at the beginning of mass transfer to the WD. The mass was reduced, by the process of mass transfer to the WD, to a value close to the present one. There is little mass stripping and energy input in the explosion, due to the compactness of the star. Another possibility might be that MV-G272 was quite more massive than MV-G272 even at the time of the explosion, a sizeable fraction of its mass having been stripped by the impact of the ejecta. It is what happens, in variable extent, to the model stars in Table 4, although none of them ends having a mass as low as that of a M1-M2 dwarf, they being too massive for that, initially. A third possibility is that MV-G272 were an M dwarf already, at the start of mass transfer. The WD should then have been quite massive. M dwarfs have never been favourites as possible SN Ia companions. They would transfer H-rich material to the mass-accreting WD at a slow rate, so giving rise to nova-like outbursts, these expelling most of the accreted mass. Wheeler (2012), however, has presented a model in which the combined magnetic fields of the WD and of the M star lock them together. A kind of *magnetic bottle* would then form and channel the mass transfer, so the WD would be accreting matter through a limited polar area. Accretion rates would be enhanced due to the luminosity of that hot spot acting on the M-dwarf end of the bottle, mixing inhibited by the magnetic field, and the accreted material kept hot, thus avoiding thermonuclear runaway outbursts. Not being spun-up by the accretion, the WD would be slowly rotating. Given the high numbers of M dwarfs, this mechanism might contribute to the observed SNe Ia rates. A fourth and last possibility is, of course, that star MV-G272 were unrelated to the SNR G272.2-3.2, its high velocity being due to past interactions with other stars, but then its path within the remnant would be a most extraordinary coincidence. We have examined several possibilities. Explanations for high-velocity stars include disruption of a close binary by the supermassive black hole at the center of the Galaxy,

with capture of a member and ejection of the other; similar three-body interaction involving a black hole at the center of a globular cluster; tidal shredding of dwarf galaxies or ejection from a nearby galaxy. None of these mechanisms is likely to impart high velocity along the Galactic plane. Dynamical interaction between groups of massive stars leading to binary disruption has also been proposed, and that would happen in the disk, but no low-mass stars like MV-G272 would be ejected. There is no stellar stream towards the site of the SNR. There is no pattern of ejected stars from a globular cluster inside the SNR and its position is far away from the supermassive black hole at the center of the Galaxy.

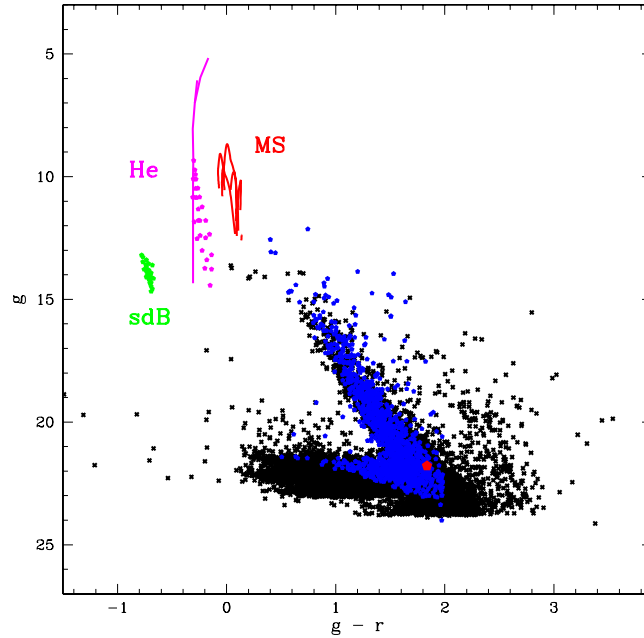


Figure 13. g vs $g - r$ magnitudes, at the distance of the SNR G272.2-3.2 (taken here as 2 kpc), of the post-explosion evolutionary tracks of MS (red) and He (magenta) star companions (from Pan et al. 2014a) and location of possible sdB companions (green) (from Meng & Li 2019), compared with our sample of stars (blue filled pentagons) from *Gaia* EDR3 and with the larger sample from the *DECaPS* survey (black crosses), covering the same area of the sky but with no constraints on distance there. The stars have been dereddened as discussed in Section 5. The red dot marks the position of star MV-G272. Due to the scale of the plot here, details of the MS evolutionary tracks are shown in Figure 14 only.

9. OTHER HIGH-PROPER MOTION STARS

Although our initial exploration of the SNR G272.2-3.2 has produced a good candidate to be the surviving companion of the exploding WD that produced the remnant, one may wonder whether a more extended search would produce some other candi-

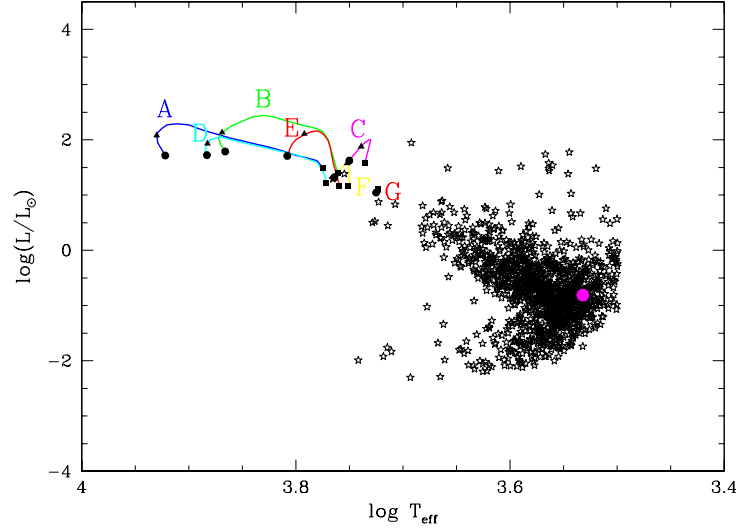


Figure 14. The HR diagram of the stars of our sample, compared with the theoretical evolutionary paths of Pan et al. (2014a) for main-sequence star companions of SNe Ia after the explosion. The evolutionary tracks cover from the time the SN Ia companions recover hydrostatic equilibrium after being impacted by the SN ejecta to 9,000 years later. The 100, 500, 3,000 and 9,000 yr post-explosion stages are marked by filled squares, stars, triangles and circles, respectively. Star MV-G272 is marked by a magenta dot. The stars have been dereddened as discussed in Section 5.

date, moving faster than MV-G272, as might be the case of some He star companions or of hypervelocity stars (produced by the D^6 mechanism mentioned in the Introduction). We will thus further explore the region around G272.2-3.2, in order to check for such extra possibilities.

In Section 2 and thereafter, a search radius of 11 arcmin around the centroid of SNR G272.2-3.2 has been adopted for the exploration. We remind that this radius corresponds to the angular distance covered by a star at 2 kpc from us, moving at 500 km s^{-1} for 12,000 yr, perpendicularly to the line of sight. One might now take the lower limit to the distance to G271.2-3.2 (1 kpc), the upper limit to its age (12,000 yr) again and include stars with tangential velocities of up to $1,000 \text{ km s}^{-1}$ (possible He star companions): a search radius of 42.2 arcmin results (almost four times that used for our initial search). We have also made such extended exploration. In Figure 15 we show the present and past positions (8,000 yr ago) of the 9 stars with total proper motions larger than that of star MV-G272, in the new area. We clearly see, from the

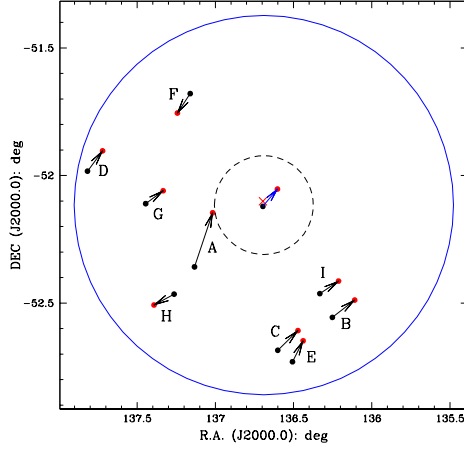


Figure 15. The 9 stars (labelled A-I), with total proper motions higher than that of MV-G272 and located between 11 arcmin and 42.2 arcmin from the centroid of the 272.2-3.2 SNR (marked with a red cross). The dashed circle corresponds to the 11 arcmin radius. Present positions are marked with red dots and those 8,000 yr ago with black ones. The motion of star MV-G272 is shown by a blue arrow. We clearly see that none of these high-velocity stars can come from inside the SNR (approximately limited by a 9 arcmin radius). Positions and proper motions from *Gaia* EDR3 are very precise, so variations of the trajectories within the error limits would hardly be seen in the Figure.

Figure, that none of the 9 stars (whose characteristics are listed in Table 5) can have anything to do with the SNR. Stars with smaller proper motions (but still at more than 3σ above the average), located within the new ring, are not shown in Figure 15, but it is obvious that, they being located outside the 11 arcmin radius around the centroid at present, and moving more slowly across the sky than MV-G272, they can hardly even have been inside the area now covered by the remnant (which has an approximate radius of 9 arcmin only), 8,000 yr ago.

Concerning the high-proper motion stars in the extended 42.2 arcmin radius area, it must be noted that the sample comprises 54,035 stars. An estimated fraction of 0.002 of the stars in the Solar neighbourhood belong to the halo population (see Konishi et al. 2015, for instance). Thus, the sample should include ~ 100 of them, with velocities of at least 220 km s^{-1} relative to the Local Standard of Rest (Du et al. 2018). From its metallicity we know that MV-G272 is not one of these.

A possible scenario for the production of SNe Ia is, as we said in the Introduction, the *dynamically driven double-degenerate, double-detonation* scenario (D⁶) (Shen & Moore 2014; Shen & Schwab 2017; Shen et al. 2018). In this scenario, detonation of a He layer at the surface of the more massive, mass-accreting WD induces, by compression, its whole detonation. That would happen when no much mass has yet

Table 5. The 9 stars with total proper motions larger than that of MV-G272, within the 42.2 arcmin radius from the centroid of G272.2-3.2.

Star	RA (deg)	DEC (deg)	d (kpc)	μ_α^* (mas yr ⁻¹)	μ_δ (mas yr ⁻¹)	v_{tan} (km s ⁻¹)
A	137.017	-52.146	$2.11^{+*}_{-1.31}$	-25.641	76.381	807^{+*}_{-501}
B	136.109	-52.488	$1.30^{+0.65}_{-0.32}$	-39.558	30.548	308^{+155}_{-75}
C	136.472	-52.608	$1.00^{+0.36}_{-0.20}$	-35.620	34.783	236^{+85}_{-47}
D	137.720	-51.903	$2.96^{+*}_{-1.94}$	-26.766	35.898	629^{+*}_{-412}
E	136.439	-52.648	$1.87^{+1.76}_{-0.61}$	-18.969	37.134	370^{+349}_{-120}
F	137.242	-51.755	$1.19^{+11.48}_{-0.56}$	22.633	-34.213	232^{+2236}_{-109}
G	137.333	-52.060	$1.43^{+2.40}_{-0.55}$	-33.587	22.790	276^{+462}_{-106}
H	137.392	-52.507	$1.03^{+1.54}_{-0.38}$	35.488	-19.089	197^{+294}_{-73}
I	136.212	-52.414	$2.57^{+*}_{-1.83}$	-32.943	22.413	486^{+*}_{-346}

been transferred from the less massive WD, which has not been tidally disrupted. It would, therefore, be ejected from the system at its orbital velocity. The system being extremely compact, the velocity should be very high ($> 1,000 \text{ km s}^{-1}$). In fact, three objects have been found, in the *Gaia* EDR2, moving at $1,000\text{--}3,000 \text{ km s}^{-1}$, which might be former WD companions in a pre-SN system (Shen et al. 2018).

Since SNR G272.2–3.2 is comparatively young, even a possible hypervelocity former companion of the SN cannot have traveled very far. Even moving at $3,000 \text{ km s}^{-1}$, perpendicularly to the line of sight, for 12,000 yr, its trajectory on the sky, assuming a distance of 2 kpc, would only reach 0.87° away from the site of the explosion. Thus, exploring the region up to a full degree from the centroid of the SNR is enough to catch any possible hypervelocity object produced by the explosion.

This new exploration has produced a sample of 112,704 stars, none of them with a total proper motion larger than that of star A in Table 5 and Figure 15. All the new high-velocity stars are outside the previously explored 11 arcmin radius, so they can in no way have originated from the SNR.

To be exhaustive, one can take a distance of 1 kpc, with the same tangential velocity of $3,000 \text{ km s}^{-1}$. That gives a radius of 2.1 degrees. The sample then comprises 514,072 stars, and again there is no star with total proper motion surpassing that of star A.

From a *Goodman* spectrum, star A (*Gaia* EDR3 5323871314998012928) is a MV1-M2V star, with solar metallicity. Although, due to the direction of its motion (see Figure 15), it can not have originated from inside the SNR G272.2-3.2, its tangential velocity, if it were at a distance of 2.11 kpc (see Table 5), would be of $\sim 807 \text{ km s}^{-1}$ (with a large error propagated from that on the parallax). From a *MIKE* spectrum (see Figure 16) we have measured its radial velocity, which is only of $v_{helio} = 57.5 \pm 0.4 \text{ km s}^{-1}$ or $v_{LSR} = 42.2 \pm 0.4 \text{ km s}^{-1}$. We thus think that star A is at a distance close to its lower limit in Table 5, which places its total velocity well below the range of the hypervelocity stars.

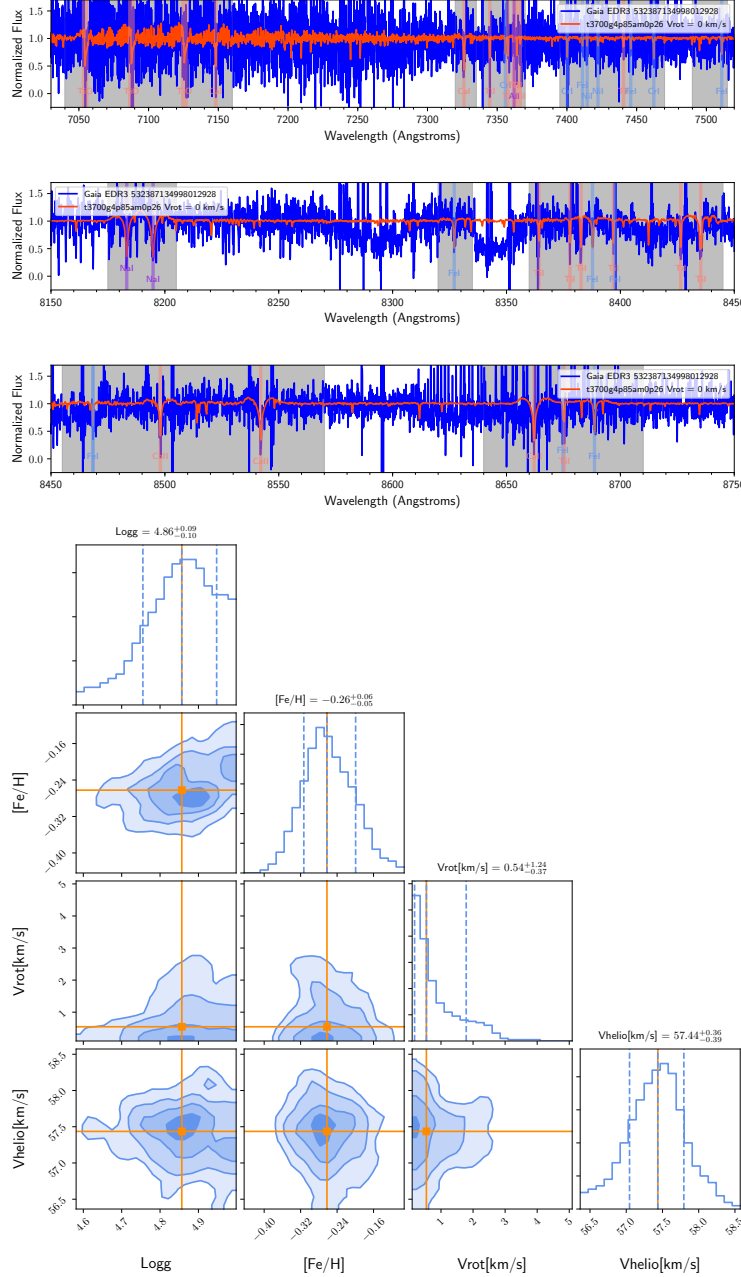


Figure 16. *MIKE* spectrum of *Gaia* EDR3 532387134998012928 (upper panel) and posterior distributions of stellar parameters and metallicity (lower panel).

A relevant question is whether hypervelocity stars like those identified by Shen et al. (2018) would be detectable at the distance of the SNR G272.2–3.2. Two of them, labelled D6–1 and D6–3 in their Table 1, are at distances of 2.1–2.3 kpc and have *Gaia* magnitudes G of 17.4–18.3, so they would have clearly been seen in our survey. As for D6–2 (LP 398–9), it is at a distance $d = 0.84 \pm 0.04$ kpc only (from this last reference), and has $G = 16.97$ mag. So, relocated at 2 kpc (the mean distance of our survey), it would still have $G = 18.85$ mag and be also detected. In addition, it has been associated with a $\sim 10^5$ yr old SNR. And the evolution of a WD after being

impacted, heated and bloated by the SN ejecta, should be cooling, contracting and fading, so at only 12,000 yr (the upper limit for the age of G272.2–3.2), such an object should be more luminous than D6–2/LP 398–9, if anything.

Therefore, we can quite confidently conclude that no hypervelocity star of the type D⁶ (Shen et al. 2028) has been produced by the explosion giving rise to G272.2–3.2.

10. SUMMARY AND CONCLUSIONS

G272.2–3.2 is the SNR of a relatively recent ($\sim 7,500$ yr old) SNIa which had been unexplored up to now in search of possible surviving companions of the SN, though being, by its distance and location in the Galaxy, accessible to observations at all wavelengths.

We have first used the parallaxes, proper motions and photometry from the *Gaia* EDR3, to explore the region within a circle of 11 arcmin radius around the centroid of the SNR and within a distance $1 \text{ kpc} \leq d \leq 3 \text{ kpc}$. That produced a sample of 3,082 stars. The surveyed area is larger than the SNR and encloses it. We then looked for kinematical signatures of a possible SNIa companion star. We also had the *Gaia* photometry, used in a subsequent step. We checked this photometry against that from the *DECaPS* survey and found complete agreement between them.

From the statistics of the proper motions of the stars in our sample, one of them, MV-G272, appears as a clear outlier, with a total proper motion 8.9σ above the mean. We checked this peculiarity against the Besançon model of the Galaxy, which confirmed it. The peculiar motion is mostly along the Galactic plane. Spectra obtained for this star have allowed us to measure its radial velocity as well. The total velocity is $v_{tot} = 256_{-70}^{+181} \text{ km s}^{-1}$, which falls within the range of velocities expected for small mass companions of SNeIa. Reconstruction, from the proper motions, of the past trajectory shows that the star, which is now near the periphery of the SNR, was at the center, 6,000–8,000 yr ago. Given the long path traced by the star, this coincidence is most significant. Such trajectory is unique among the 3,082 stars of the sample.

Spectra obtained with the *MIKE* spectrograph at the 6.5m *Clay* telescope and with the *Goodman* spectrograph at the 4.1m *SOAR* telescope, allowed the classification of MV-G272 as a M1–M2 dwarf, with solar metallicity, by comparing them with *BOSS* templates. They also showed that the extinction, in the direction of the SNR, was small, which is relevant for the photometry. The star thus has a mass $M = 0.44\text{--}0.50 M_{\odot}$ and radius $R = 0.446\text{--}0.501 R_{\odot}$. There is agreement between the measured total velocity of MV-G272 and the ejection velocity of a M1–M2 dwarf in close orbit with a $1.4 M_{\odot}$ WD, when the binary is disrupted by a SNIa explosion.

The spectrum obtained with the *MIKE* spectrograph at the 6.5m *Clay* telescope has allowed to establish the values of the stellar parameters of MV-G272 and also to make a chemical analysis of its surface through synthetic spectra analysis (see section 6). We have then $T_{eff} = 3,800 \text{ K}$ (the range can be 3,600–3,850 K, given the systematic uncertainties), $\log g = 4.46$ and metallicity about solar: $[\text{Fe}/\text{H}] = -0.32$ (with 0.3 dex

in error). We also looked for signs of overabundances of Fe-peak elements coming from the SN ejecta, but systematic uncertainties preclude any conclusion. In any case, a M1-M2 dwarf being almost fully convective, a strong dilution of this material should be expected.

The *Gaia* EDR3 photometry, together with the estimate of the reddening and the knowledge of the distances, allows to construct the color-magnitude and the HR diagrams of the stars of our sample. They are compared with the existing models of the evolution of proposed SNIa companions. That has allowed to discard the presence of RGs, He stars and sdB companion stars in our sample.

The models for MS companions are more luminous and hotter than the sampled stars. MV-G272 is fainter and cooler than any of the model stars, but all the models are for much more massive stars, so the comparison is not significant.

To be exhaustive, the possibility that the SN were produced through the D^6 mechanism has been checked by the exploration of a circle with 2.1 degree radius around the SNR. None has been found.

We have examined all evolutionary paths that might have led to the SNIa that produced SNR G272.2-3.2.

We have a very kinematically peculiar star, MV-G272 with all signs of having been ejected by a explosion taking place at the center of a SNIa SNR. Such characteristics make it unique. Although its being a late-type, small star could come as a surprise, the evidence in its favour is very solid, coming from its kinematics and its trajectory inside the SNR.

In conclusion, we have found a possible companion star of the SNIa that resulted in SNR G272.2-3.2, with much evidence in its favor. This would be the case, therefore, of a SD scenario involving a M dwarf star. Since, from the chemical abundances in its ejecta, the explosion that gave rise to SNR G272.2-3.2 was a normal SNIa and M dwarfs are the most abundant stars in the Galaxy, that opens up the prospect for many SNeIa to have the same origin.

Based on observations obtained at the Southern Astrophysical Research (SOAR) telescope (NOIRLab Prop. 2022A-606104), which is a joint project of the Ministerio da Ciencia, Tecnología e Innovaciones (MCTI/LNA) do Brasil, the US National Science Foundation's NOIRLab, the University of North Carolina at Chapel Hill (UNC), and Michigan State University (MSU). We are grateful to the SOAR staff for their help in performing the observations of this project.

This paper includes data gathered with the 6.5 meter Magellan Telescopes located at Las Campanas Observatory, Chile.

This work has made extensive use of the *Gaia* EDR3. *Gaia* data are being processed by the *Gaia* Data Processing and Analysis Consortium (DPAC). Funding for the DPAC is provided by national institutions, in particular the institutions participating in the *Gaia* MultiLateral Agreement (MLA). The *Gaia* mission website is <https://www.cosmos.esa.int/gaia>. The *Gaia* archive website is

<https://archives.esac.esa.int/gaia>. This work was (partially) funded by the Spanish Ministry of Science and Innovation (MICINN), the Agencia Estatal de Investigación (AEI) 10.13039/501100011033 and by "ERDF A way of making Europe" by the "European Union" through grants RTI2018-095076-B-C21 and PID2021-122842OB-C21, and the Institute of Cosmos Sciences University of Barcelona (ICCUB, Unidad de Excelencia 'María de Maeztu') through grant CEX2019-000918-M.

PR-L also acknowledges support from grant PGC2018-095157-B-I00, from the MICINN. JIGH acknowledges financial support from the MICINN PID2020-117493GB-I00, and also from the Spanish MICINN 2013 Ramon y Cajal program RYC-2013-14875. R.C acknowledges financial support from grant PGC2018-095157-B-I00 from Spanish MICINN. L.G. acknowledges financial support from the Spanish MICINN, AEI 10.13039/501100011033, and the European Social Fund (ESF) "Investing in your future" under the 2019 Ramón y Cajal program RYC2019-027683-I and the PID2020-115253GA-I00 HOSTFLOWS project, from Centro Superior de Investigaciones Científicas (CSIC) under the PIE project 20215AT016, and the program Unidad de Excelencia María de Maeztu CEX2020-001058-M.

PRL would like to thank Evan Bauer and Warren Brown at the Harvard-Smithsonian Center for Astrophysics, and Christian Knigge from the University of Southampton, for conversations. The authors would like to thank the anonymous referee for the valuable comments on the manuscript.

References

- Bauer, E.B., White, C.J., & Bildsten, L. 2019, *ApJ*, 887, 68
- Bedin, L.R., Ruiz-Lapuente, P., González Hernández, J.I., et al. 2014, *MNRAS*, 439, 354
- Bernstein, R., Sackett, S. A., Gunnels, S. M., et al. 2003, *SPIE*, 4841, 1694. doi:10.1117/12.461502
- Branch, D., & Wheeler, J.C. 2017, *Supernova Explosions* (Berlin, Springer)
- Castelli, F., & Kurucz, R. L. 2003, *Modelling of Stellar Atmospheres*, 210, A20
- Clemens, J.C., Crain, J.A., & Anderson, R. 2004, *SPIE*, 5492, 455
- Di Stefano, R., Voss, R., & Claeys, J.S.W. 2011, *ApJL*, 738, L1
- Du, C., Li, H., Liu, S., Donlon, T., & Newberg, H.J. 2018, *ApJ*, 863, 87
- Duncan, A.R., Stewart, R.T., Campbell-Wilson, D., Haynes, R.F., Aschenbach, R., & Jones, K.L. 1997, *MNRAS*, 289, 77
- Edwards, Z.I., Pagnotta, A., & Schaefer, B.E. 2012, *ApJ*, 747, L19
- Eggleton, P.P. 1983, *ApJ*, 268, 368
- Foreman-Mackey, D., Hogg, D. W., Lang, D., et al. 2013, *PASP*, 125, 306. doi:10.1086/670067
- González Hernández, J.I., Ruiz-Lapuente, P., Filippenko, A.V., et al. 2009, *ApJ*, 691, 1

- González Hernández, J.I., Ruiz-Lapuente, P., Tabernero, H.M., et al. 2012, *Natur*, 489, 533
- Greiner, J., & Egger, R. 1993, *IAU Circ. No.* 5709
- Greiner, J., Egger, R., & Aschenbach, B. 1994, *A&A*, 286, L35
- Han, Z. 2008, *ApJL*, 677, L109
- Harrus, I.H., Slane, P.O., Smith, R.K., & Hughes, J.P. 2001, *ApJ*, 552, 614
- Hayden, B., Rubin, D., Boone, K., et al. 2021, *ApJ*, 912, 87
- Houdashelt, M. L., Bell, R. A., Sweigart, A. V., & Wing, R. F. 2000, *AJ*, 119, 1424
- Iben, I., Jr., & Tutukov, A.V. 1984, *ApJS*, 54, 355
- Jenkins, J.S., Ramsey, L.W., Jones, H.R.A., et al. 2009, *ApJ*, 704, 975
- Jordi, C., Gebran, M., Carrasco, J. M., et al. 2010, *A&A*, 523, A48
- Justham, S. 2011, *ApJL*, 730, L34
- Kashi, A., & Soker, N. 2011, *MNRAS*, 417, 1466
- Kamitsukasa, F., Koyama, K., Nakajima, H., et al. 2016, *PASJ*, 685, 7
- Kelson, D.D. 2003, *PASP*, 115, 688
- Kelson, D.D., Illingworth, G.D., van Dorkum, P.G., & Franx, M. 2000, *ApJ*, 531, 159
- Kerzendorf, W.E., Schmidt, B.P., Asplund, M., et al. 2009, *ApJ*, 701, 1665
- Kerzendorf, W.E., Schmidt, B.P., Laird, J.B., et al. 2012, *ApJ*, 759, 7
- Kerzendorf, W.E., Yong, D., Schmidt, B.P., et al. 2013, *ApJ*, 774, 99
- Kerzendorf, W.E., Childress, M., Scharwächter, J., Do, T., & Schmidt, B.P. 2014, *ApJ*, 782, 27
- Kerzendorf, W.E., Long, K.S., Winkler, P.F., & Do, T. 2018a, *MNRAS*, 479, 5696
- Kerzendorf, W.E., Strampelli, G., Shen, K.J., et al. 2018b, *MNRAS*, 479, 192
- Kesseli, A.Y., West, A.A., Veyette, M., et al. 207, *ApJS*, 230, 16
- Kesseli, A.Y., West, A.A., Veyette, M., et al. 2020, *Astrophysics Source Code Library*, ascl:2002.011. PyHammer: Python spectral typing suite.
- Konishi, M., Hiroshi, S., Sumi, T., et al. 2015, *PASJ*, 67, 1
- Kurucz, R. L., Furenlid, I., Brault, J., et al. 1984, *National Solar Observatory Atlas, Sunspot, New Mexico: National Solar Observatory*, 1984
- Leahy, D.A., Ranasinghe, S., & Gelowitz, M. 2020, *ApJS*, 248, 16
- Li, C.-J., Chu, Y.-H., Gruendl, R.A., et al. 2017, *ApJ*, 836, 8
- Li, C.-J., Kerzendorf, W.E., Chu, Y.-H., et al. 2019, *ApJ*, 886, 99
- Litke, K.C., Chu, Y.-H., Holmes, A., et al. 2017, *ApJ*, 837, 111
- Liu, Z.-W., Pakmor, R., Seitzzahl, I.R., et al. 2013a, *ApJ*, 774, 37
- Liu, Z.-W., Pakmor, R., Röpke, F.K., et al. 2013b, *A&A*, 554, A109
- Liu, Z.-W., Röpke, F.K., & Zeng, Y. 2022, *ApJ*, 928, 146
- Livne, E. 1990, *ApJL*, 345, L53
- Livne, E., & Arnett, D. 1995, *ApJ*, 452, 62
- Lopez, L.A., Ramirez-Ruiz, E., Hupferkoth, D., Badenes, C., & Pooley, D.A. 2011, *ApJ*, 732, 114

- Marfil, E., Tabernero, H. M., Montes, D., et al. 2021, *A&A*, 656, A162.
doi:10.1051/0004-6361/202141980
- Marietta, E., Burrows, A., & Fryxell, B. 2000, *ApJS*, 128, 615
- McEntaffer, R.L., Grieves, N., DeRoo, C.L., & Brantseg, T. 2013, *ApJ*, 774, 120
- Maoz, D., Mannucci, F., & Nelemans, G. 2014, *ARA&A*, 52, 107
- McCutcheon, C., Zeng, Y., Liu, Z.-W., Izzard, R.G., Pan, K.C., Chen, H.-L., & Han, Z. 2022, *MNRAS*, 514, 4078
- Meng, X., & Li, J. 2019, *MNRAS*, 482, 5651
- Meng, X.-C., & Luo, Y.-P. 2021, *MNRAS*, 507, 4603
- Nomoto, K. 1982, *ApJ*, 253, 798
- Pakmor, R., Röpke, F.K., Weiss, A., & Hillebrandt, W. 2008, *A&A*, 489, 943
- Pakmor, R., Kromer, M., Taubenberger, S., et al. 2012, *ApJL*, 747, L10
- Pan, K.-C., Ricker, P.M., & Taam, R.E. 2012a, *ApJ*, 750, 151
- Pan, K.-C., Ricker, P.M., & Taam, R.E. 2012b, *ApJ*, 760, 21
- Pan, K.-C., Ricker, P.M., & Taam, R.E. 2013, *ApJ*, 773, 49
- Pan, K.-C., Ricker, P.M., & Taam, R.E. 2014, *ApJ*, 792, 71
- Passeger, V. M., Bello-García, A., Ordieres-Meré, J., et al. 2022, *A & A*, 658, A194
- Pecaut, M.J., & Mamajek, E.E. 2013, *ApJS*, 208, 9
- Perlmutter, S., Aldering, G., Goldhaber, G., et al. 1999, *ApJ*, 517, 565
- Podsiadlowski, P. 2003, arXiv:0303.660
- Rau, S.-J., & Pan, K.-C. 2022, *ApJ*, 933, 38
- Reiners, A., Zechmeister, M., Caballero, J. A., et al. 2018, *A&A*, 612, A49.
doi:10.1051/0004-6361/201732054
- Riess, A.G., Filippenko, A.V., Challis, P., et al. 1998, *AJ*, 116, 1009
- Rose, B.M., Rubin, D., Cikota, A., et al. 2020, *ApJL*, 896, L4
- Rosswog, S., Kasen, D., Guillochon, J., & Ramirez-Ruiz, E. 2009, *ApJL*, 705, L128
- Ruiz-Lapuente, P. 1997, *Sci*, 276, 1813
- Ruiz-Lapuente, P. 2004, *ApJ*, 612, 357
- Ruiz-Lapuente, P. 2014, *NewAR*, 62, 15
- Ruiz-Lapuente, P. 2019, *NewAR*, 85, 101523
- Ruiz-Lapuente, P., Comerón, F., Méndez, J., et al. 2004, *Nature*, 431, 1069
- Ruiz-Lapuente, P., Damiani, F., Bedin, L., et al. 2018, *ApJ*, 862, 124
- Ruiz-Lapuente, P., González Hernández, J.I., Mor, R., et al. 2019, *ApJ*, 870, 135
- Sezer, & Gök, F. 2012, *MNRAS*, 421, 3538
- Sánchez-Ayaso, E., Combi, J.A., Bocchino, J.F., et al. 2013, *A&A*, 552, A52
- Schaefer, B.E., & Pagnotta, A. 2012, *Natur*, 481, 164
- Shappee, B.J., Kochanek, C.S., & Stanek, K.Z. 2013, *ApJ*, 765, 150
- Shen, K.J., & Moore, K. 2014, *ApJ*, 797, 46
- Shen, K.J., & Schwab, J. 2017, *ApJ*, 834, 180
- Shen, K.J., Boubert, D., Gänsicke, B.T., et al. 2018, *ApJ*, 865, 15
- Shields, J.V., Kerzendorf, W., Hosek, Jr., M.W., et al. 2022, *ApJL*, 933, L31

Soker, N. 2013, in IAU Symp. 281, Binary Paths to Type Ia Supernova Explosions, ed. R. Di Stefano, M. Orio, & M. Moe (Cambridge UK, Cambridge Univ. Press), 72.

Tabernero, H. M., Marfil, E., Montes, D., et al. 2021, Astrophysics Source Code Library. ascl:2111.016. SterParSyn: Stellar atmospheric parameters using the spectral synthesis method.

Tabernero, H. M., Marfil, E., Montes, D., et al. 2022, A&A, 657, A66. doi:10.1051/0004-6361/202141763

van Dokkum, P.G. 2001, PASP, 113, 1420

Wang, B., & Han, Z. 2012, NewAR, 56, 122

Webbink, R.F. 1984, ApJ, 277, 355

Wheeler, J.C. 2012, ApJ, 758, 123

Whelan, J., & Iben, I., Jr. 1973, ApJ, 186, 1007

Xiang, Y., & Jiang, Z. 2021, ApJ, 918, 24

Yamaguchi, H., Badenes, C., Petre, R., et al. 2014, ApJL, 785, L2

APPENDIX

MIKE Spectrum Fits

The analysis of the combined high-resolution MIKE spectrum ($R \sim 28,000$) of the target Star MV-G272 is depicted in Fig. 17, where we have zoomed into several spectral regions from the whole spectral range shown in Fig. 12. We also display the residuals the observed minus computed synthetic spectra (O-C) to compare the observations and the model. We see some remaining features corresponding to residuals coming from sky subtraction and the telluric spectrum.

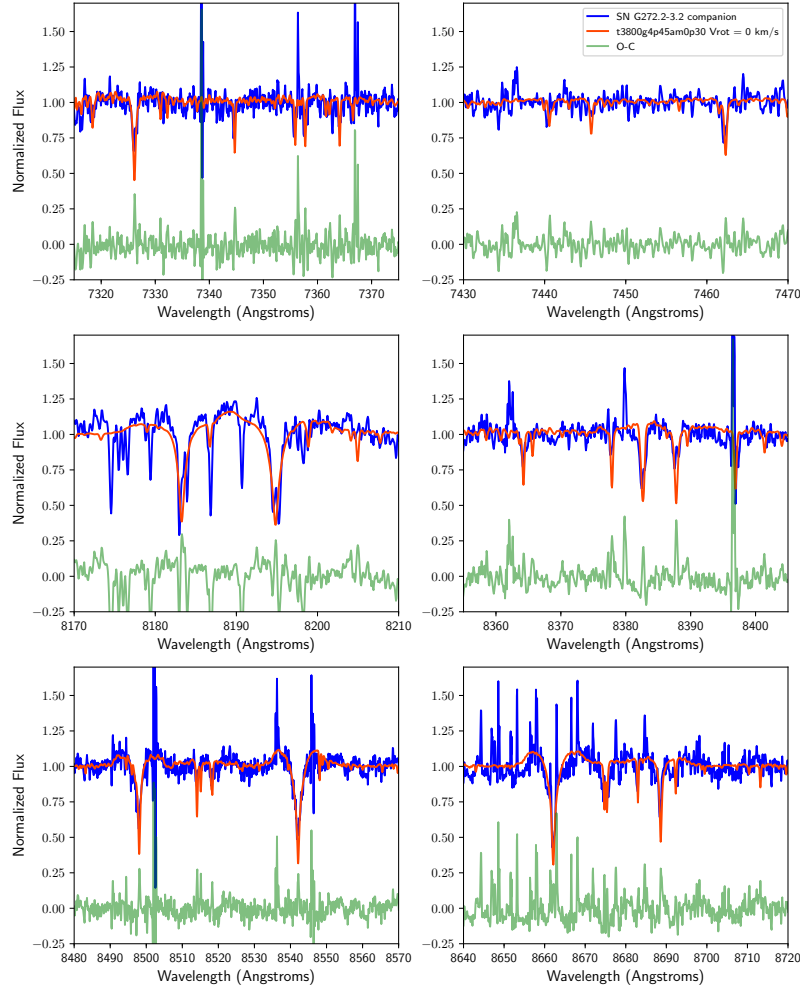


Figure 17. Comparison of the observed *MIKE* spectrum of MV-G272 with the fitted spectrum, in the wavelength ranges 7,320-7,370 Å and 7,430-7,470 Å (upper panel), 8,170-8,210 Å and 8,360-8,400 Å (middle panel) and 8,480-8,570 Å and 8,640-8,720 Å (lower panel).

We have tested our stellar parameter and metallicity determination using high-resolution CARMENES-VIS spectra (Reiners et al. 2018) with a resolution of $R \sim 94,600$, degraded to a resolving power of $R \sim 28,000$. We chose two M1V stars Karmn J00183+440 (GX And) and Karmn J05415+534 (HD 233153), with injected white noise down to $S/N \sim 10$, as explained in Section 6.

A1. CARMENES Spectra

We display in Fig. 18 and 19, the resulting spectra of these two M dwarf stars compare with a synthetic spectrum in the same spectral range as the MIKE spectrum of the target Star MV-G272 display in Fig. 12.

S

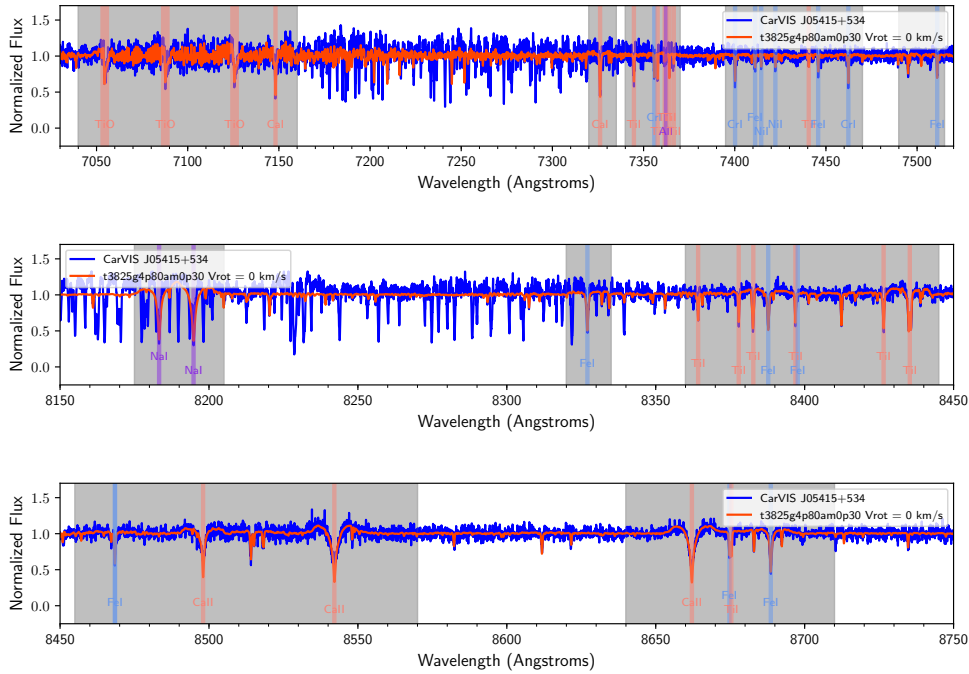


Figure 18. Degraded and normalized CARMENES VIS 1D spectrum of star Karmn J05415+534 (HD 233153), corrected for barycentric radial velocity, degraded to a resolving power of $R \sim 28,000$, with a signal-to-noise ratio of ~ 15 at 7400 Å, and normalized to unity using a running mean filter with a width of 200 pixels at 0.069 Å per pixel. We also display an interpolated SYNPLE synthetic spectrum with the stellar parameters $T_{\text{eff}} = 3825$ K, $\log g = 4.80$ and and metallicity $[\text{Fe}/\text{H}] = -0.3$. The regions used to estimate the metallicity are shown in grey and the different lines used for chemical analysis are also highlighted.

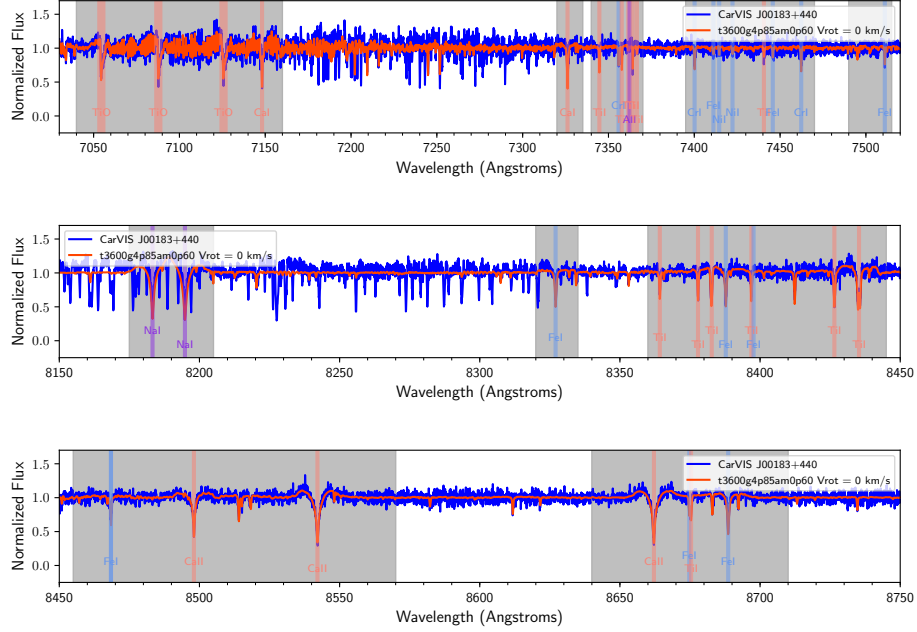


Figure 19. Normalized and degraded CARMENES VIS 1D spectrum of star Karmn J00183+440 (GX And), corrected for barycentric radial velocity, degraded to a resolving power of $R \sim 28,000$, with a signal-to-noise ratio of ~ 15 at 7400 \AA , and normalized to unity using a running mean filter with a width of 200 pixels at 0.069 \AA per pixel. We also display an interpolated SYNPLE synthetic spectrum with the stellar parameters $T_{\text{eff}} = 3600 \text{ K}$, $\log g = 4.85$ and and metallicity $[\text{Fe}/\text{H}] = -0.6$. The regions used to estimate the metallicity are shown in grey and the different lines used for chemical analysis are also highlighted.